

Atomic Proximal Policy Optimization for Electric Robo-Taxi Dispatch and Charger Allocation

Jim Dai

Operations Research and Information Engineering, Cornell University, jd694@cornell.edu

Manxi Wu

Department of Civil and Environmental Engineering, University of California, Berkeley, manxiwu@berkeley.edu

Zhanhao Zhang

Operations Research and Information Engineering, Cornell University, zz564@cornell.edu

Abstract

Pioneering companies such as Waymo have deployed robo-taxi services in several U.S. cities. These robo-taxis are electric vehicles, and their operations require the joint optimization of ride matching, vehicle repositioning, and charging scheduling in a stochastic environment. We model the operations of the ride-hailing system with robo-taxis as a discrete-time, average-reward Markov Decision Process with an infinite horizon. As the fleet size grows, dispatching becomes challenging, as both the system state space and the fleet dispatching action space grow exponentially with the number of vehicles. To address this, we introduce a scalable deep reinforcement learning algorithm, called Atomic Proximal Policy Optimization (Atomic-PPO), that reduces the action space using atomic action decomposition. We evaluate our algorithm using real-world NYC for-hire vehicle trip records and measure its performance by the long-run average reward achieved by the dispatching policy, relative to a fluid-based upper bound. Our experiments demonstrate the superior performance of Atomic-PPO compared to benchmark methods. Furthermore, we conduct extensive numerical experiments to analyze the efficient allocation of charging facilities and assess the impact of vehicle range and charger speed on system performance.

1 Introduction

Robo-taxi services have been deployed in several U.S. cities, including San Francisco, Phoenix, and Los Angeles [1]. Efficiently operating electric robo-taxi fleet is challenging due to the stochastic and spatiotemporal nature of trip demand, combined with the need to schedule battery charging under limited charging infrastructure. Inefficient operations could render vehicles unavailable during high-demand periods, leading to decreased service quality, reliability issues, and revenue loss.

In this work, we model the electric robo-taxi fleet operations problem as a Markov decision process with discrete state and action space. The state of the system records the spatial distribution

of vehicles, their current tasks, active trip requests, and the availability of chargers. Based on the state, the system makes fleet dispatch decisions to fulfill trips, reposition vehicles, and schedule charging, with each action associated with certain reward or cost. Our goal is to find a fleet dispatching policy that maximizes the long-run average reward over an infinite time horizon.

The challenge of computing the fleet dispatching policy arises from the high-dimensionality of the state and action space. Since the state space represents all possible distributions of vehicle statuses and the action space includes all feasible vehicle assignments, both grow exponentially with fleet size. We develop a scalable deep reinforcement learning (RL) algorithm, which we refer as atomic proximal policy optimization (Atomic-PPO). The efficiency of Atomic-PPO is accomplished by decomposing the dispatching of the entire fleet into the sequential assignment of atomic actions – tasks such as trip fulfillment, reposition, charge or pass (i.e. no new task) – to individual vehicles, which we refer to as “atomic action decomposition”. The dimension of the atomic action space equals to the number of feasible tasks that can be assigned to an individual vehicle. Hence, the atomic action decomposition reduces the action space from being exponential in fleet size to being a constant, significantly reducing the complexity of policy training. We integrate our atomic action decomposition into a state-of-art RL algorithm, the Proximal Policy Optimization (PPO) [2], which possesses the monotonic policy improvement guarantee and has proven to be effective in policy optimization across various applications [3, 4, 5, 6, 7]. We approximate both the value function and the policy over atomic actions using neural networks in the Atomic-PPO training. We also further reduce the dimensionality of the state representation by clustering vehicle battery levels and grouping trip requests based on their origins.

Furthermore, we derive an upper bound on the optimal long-run average reward using a fluid-based linear program (LP) (see Theorem 1). The fluid limit is attained as the fleet size approaches infinity, with both trip demand volume and the number of chargers scaling up proportionally to the fleet size. This reward upper bound is useful for assessing the optimality gap of the policy trained by our algorithm in numerical experiments, as we will discuss next.

We evaluate the performance of our Atomic PPO algorithm using the NYC For-Hire Vehicle dataset [8] in Manhattan area with a fleet size of 300, which is comparable to the fleet size deployed in a city by Waymo [9]. The fleet size is approximately 5% of the for-hire vehicles in Manhattan area and we scale down the trip demand accordingly. Furthermore, our simulation incorporates the nonlinear charging rate, time-varying charging, repositioning costs, and trip rewards. We benchmark the performance of our fleet dispatching policy against a fluid-based reward upper bound and two heuristic policies. Specifically, we compute the ratio between the reward achieved by our policy and the fluid-based upper bound. This ratio serves as a conservative estimate—that is, a lower bound—of the actual optimality ratio achieved by our learning algorithm. Additionally, the first benchmark heuristic is computed by applying randomized rounding to the fractional solution obtained from the fluid-based LP. The second heuristic is the power-of-k dispatching policy that selects k closest vehicles for a trip request and matches the request with the vehicle that has the highest battery

level [10].¹

In our baseline setting, we assume that there are abundant number of DC Fast chargers (75 kW) in all regions. Our Atomic-PPO beats both benchmarks in terms of total reward by a large margin. In particular, Atomic-PPO can achieve 91% of fluid upper bound, while the power-of-k dispatching and the fluid policy can only achieve 71% and 43% of fluid upper bound, respectively. Moreover, our Atomic-PPO can achieve a near-full utilization of fleet for trip fulfillment during rush hours, while both benchmark policies have a significant number of vehicles idling at all time steps. The training of our Atomic-PPO is highly efficient – the training for 300 vehicle fleet can be completed within 3 hours using 30 CPUs.

Additionally, we investigate the impact of charging facility allocation, vehicle range, and charging rate on the long-run average reward. We find that uniformly allocating chargers across all regions is inefficient, and requires 30 chargers (10% of the fleet size) to achieve a long-run average reward comparable to the case with abundant chargers. In contrast, allocating chargers based on ridership patterns achieves similar performance with only 15 chargers (5% of the fleet size). Additionally, our experiments demonstrate that fast charging speed plays a crucial role in achieving high rewards, whereas increasing vehicle range has no significant impact on reward. This is because fast chargers significantly reduce the time needed to recharge the battery, thereby lowering the opportunity cost of missed trip requests. On the other hand, vehicle range is less critical since most trips are short in Manhattan.

Related Literature. The problem of optimal fleet dispatch has been extensively studied in the context of ride-hailing systems, with the majority focuses on gasoline vehicles (and thus no need for scheduling charging) and several recent works on EVs [10, 13, 14, 15, 16, 17, 18, 19, 20, 21, 22, 23, 24, 25, 26, 27, 28, 29, 30, 31, 32, 33, 34, 35, 36, 37, 38]. The methods adopted in these papers fall into one of the three categories: (1) deterministic optimization methods; (2) queueing-based analysis; and (3) deep reinforcement learning.

(1) Deterministic optimization. The first category of works models the ride hailing system as a deterministic system, where all future trip arrivals are known. In deterministic systems, the optimal fleet dispatch can be formulated as a linear program [14] or mixed integer programs (MIP) [16, 15, 19, 39, 20, 23, 26, 28, 30, 32, 34]. These methods cannot be applied to settings with uncertain trip demand.

(2) Queueing-Based Analysis. The second category of related work models ride-hailing systems as queueing systems. Some studies adopt a closed queueing system approach [40, 41, 42, 43, 44],

¹The power-of-k dispatching policy is rooted in the load-balancing literature [11, 12]. In the load-balancing context, the power-of-k uniformly samples k number of queues and then routes the job to the shortest queue among them. The paper [10] demonstrates that under the assumption that all trip requests and charging facilities are uniformly distributed across the entire service area, the power-of-k dispatching policy can achieve the asymptotically optimal service level. We note that this assumption is restrictive and is not satisfied in our setting.

where drivers remain in the system indefinitely. Others employ an open queueing system framework [10, 22, 45, 46, 47, 48], where drivers dynamically enter and exit the system.

Notably, all of these studies except for Varma et al. [10] focus on gasoline vehicle dispatching and do not consider charging constraints. Moreover, most assume time-homogeneity, with exceptions such as [46, 47, 44, 48], which incorporate time-varying dynamics. The primary focus of this body of work has been on developing fleet control policies that are optimal under specific conditions or in the fluid limit. Our construction of a reward upper bound builds on the fluid-based analytical methods developed in this literature. However, while these policies are provably optimal as fleet size approaches infinity, their performance can suffer from significant optimality gaps when the fleet size is moderate. In particular, we find that the power-of-k policy proposed in [10] is indeed suboptimal and achieves a lower reward compared to our policy.

(3) Deep Reinforcement Learning. The third category of research uses deep reinforcement learning (RL) to train fleet dispatching policies in complex environments that incorporate both spatial and temporal demand uncertainty. For a comprehensive review of these studies, see the recent survey by [49]. Majority of studies in this category including ours model the ride-hailing system as a Markov Decision Process (MDP), where dispatch decisions are made for the entire fleet at discreet time steps. A few articles modeled the system as a semi-MDP, where decision making is triggered by trip arrival or a vehicle completing a task [18, 21, 50, 27].

Our work is distinguished from previous studies by formulating an infinite-horizon Markov Decision Process (MDP) with a long-run average reward objective. In contrast, existing research adopts either finite-horizon MDPs, where decisions are optimized over a short time frame, or infinite-horizon MDPs with discounted reward, which prioritize near-term rewards. These formulations are sufficient for modeling conventional vehicle ride-hailing systems, where daily operations effectively reset at midnight due to low demand. However, they are inadequate for systems with electric vehicle, where long-term battery management is critical. Policies trained with finite-horizon models or discounted objectives may neglect future battery need that leads to widespread battery depletion across the fleet. In scenarios where charging infrastructure is limited and cannot charge all vehicles overnight, a fleet with depleted batteries is unable to meet demand the next day. Thus, incorporating an average-reward objective in an infinite-horizon framework is essential for modeling EV operations, as it enables the optimization of steady-state battery levels and long-run system performance.

A major challenge in training fleet dispatching policies is managing the high dimensionality of state and action spaces. Most studies only focus on specific subproblems, such as ride matching, vehicle repositioning, or charging, rather than developing an integrated framework that address all these components simultaneously. A few exceptions include [31, 33, 37, 18, 36]. Our model also falls into this category as we provide a comprehensive fleet dispatch policy that jointly controls ride matching, repositioning, and charging.

To tackle the curse of dimensionality arising from the large fleet size, prior works adopted various strategies that include (i) T-step look ahead approach [51] that computes the optimal

fleet dispatching actions in the first T steps of the value iteration by solving a linear program, (ii) warm start approach [52] that initializes the fleet dispatching policy by imitation learning from mixed integer programs, (iii) restricting vehicles at the same region to take the same action [53, 54], or (iv) relaxing integral constraints and treating the fleet action as continuous variables [55, 56, 57, 36, 58, 59, 60, 61, 62]. However, T-step look ahead approach and warm start approach are still computationally challenging as they need to repeatedly solve large-scale linear programs or mixed integer programs. The remaining two approaches may incur errors that increase in the system’s complexity, especially with the integration of ride-matching, repositioning, and charging.

Another extensively studied method to reduce the dimensionality of the policy space is to use a decentralized reinforcement learning (RL) training approach [63, 64, 65, 66, 67, 68, 69, 70, 71, 72, 73, 74, 75, 24, 76, 77, 78, 79, 80, 81, 67, 82, 83, 84, 85, 86, 87, 88, 89, 25, 29, 31, 33, 37]. In this approach, vehicles are treated as homogeneous and uncoordinated agents that make independent decisions based on a shared Q-function. While the decentralized RL approach effectively reduces the policy dimension, the resulting policy is theoretically suboptimal because it fails to account for the collective impact of individual vehicle actions on state transitions and overall system reward. Our Atomic PPO algorithm addresses this issue by introducing a coordinated sequential assignment of atomic actions that incorporates state transitions after each step. Therefore, our atomic decomposition reduces the action space while ensuring the algorithm still accounts for the impact of each vehicle’s action on the system state and learns the accumulated rewards from the dispatch actions of the entire fleet in each decision epoch.

Finally, our Atomic-PPO algorithm builds on our previous conference article [90], which addressed ride matching and vehicle repositioning for conventional vehicle fleets within a finite-horizon framework. In this study, we extend the framework by incorporating charging and adopting an infinite-horizon, long-run average reward objective. Consequently, our algorithm introduces a new state reduction scheme to address these added complexities. Furthermore, we provide a theoretical upper bound on the optimal long-run average reward that serves as a benchmark for our fleet dispatching policy. Experimental results show that our algorithm achieves a reward with gap less than 10% of the theoretical upper bound while maintaining low training costs.

2 Model

2.1 The ride-hailing system

We consider a transportation network with V service regions. In this network, a fleet of electric vehicles with size N are operated by a central planner to serve passengers, who make trip requests from their origins $u \in V$ to their destinations $v \in V$. For each pair of $(u, v) \in V \times V$, we assume that the battery consumption for traveling from u to v is a constant $b_{uv} \in \mathbb{R}_{\geq 0}$. The electric vehicles are each equipped with a battery of size B , i.e. a fully charged vehicle can take trips with total battery consumption up to B . A set of chargers with different charging rates $\delta \in \Delta$ are installed in

the network, where each rate δ charger can replenish δ amount of battery to the connected vehicle in one unit of time. We denote the number of rate $\delta \in \Delta$ chargers in each region $v \in V$ as $n_v^\delta \in \mathbb{N}_{\geq 0}$.

We model the operations of a ride-hailing system as a discrete-time, average reward Markov Decision Process (MDP) with infinite time horizon. In particular, we model the system as an infinite repetition of a single-day operations, where each day $d = 1, 2, \dots$ is evenly partitioned into T number of time steps $t = 1, \dots, T$. The system makes a dispatching decision for the entire fleet at every time step of a day, which we refer to as a decision epoch. In each decision epoch (t, d) , the number of trip requests between each $u-v$ pair, denoted as $X_{uv}^{t,d}$, follows a Poisson distribution with mean λ_{uv}^t . The duration of trips from region u to region v at time t is a constant τ_{uv}^t that is a multiple of the length of a time step. Both λ_{uv}^t and τ_{uv}^t can vary across time steps in a single day, but remain unchanged across days.

When the central planner receives the trip requests, they assign vehicles to serve (all or a part of) the requests. In particular, a vehicle must be assigned to the passenger within the connection patience time $L_c \geq 0$, and a passenger will wait at most time $L_p \geq 0$ (defined as the pickup-patience time) for an assigned vehicle to arrive at their origin. Otherwise, the passenger will leave the system. Both L_p and L_c are multiples of the discrete time steps.

The central planner keeps track of the status of each vehicle by the region $v \in V$ it is currently located or heading to, remaining time to reach $\eta = 0, \dots, \hat{\tau}_v$, and remaining battery level $b = 0, \dots, B$ when reaching v . Here, $\hat{\tau}_v := \max_{u \in V, t \in [T]} \tau_{uv}^t$ is the maximum duration of any trip with destination v . We assume that the minimum time cost of all trips $\min_{u, v \in V, t \in [T]} \tau_{uv}^t$ is larger than L_p so that no vehicle can be assigned to serve more than one trip request in a single decision epoch.

A vehicle is associated with status $c = (v, \eta, b)$ if (1) it is routed to destination v , with remaining time η , and battery level b at the arrival; or (2) it is being charged at region v , with remaining charging time η , and battery level b after the charging period completes. Here, if $\eta = 0$, then the vehicle is idling at region v . Additionally, if $\eta > 0$, then the vehicle could either be taking a trip with a passenger whose destination is v , being repositioned to v , or being charged in v . Vehicle repositioning may serve two purposes: (1) to pick up the next passenger whose origin is v ; (2) to be charged or idle at region v . We note that the maximum remaining time η for trip fulfilling vehicles cannot exceed a finite number $\hat{\tau}_v + L_p$ since a vehicle is only eligible to serve a trip if the vehicle can arrive at the origin of that trip within L_p time and the maximum trip duration is $\hat{\tau}_v$. Additionally, a vehicle with status $(v, 0, b)$ can be charged at region v with rate δ if such a charger is available in v .² Charging takes J time steps. If the vehicle is charged to full within J time steps, then it will remain connected to the charger and idle for the remaining time of the charging period. We assume that $J > L_p$ so that vehicles assigned to charge will not be assigned to serve trip requests in the same decision epoch. Let $\mathcal{C} := \{(v, \eta, b)\}_{v \in V, \eta=0, \dots, \hat{\tau}_v, b=0, \dots, B}$ denote the set of all vehicle status. The set \mathcal{C} is finite.

A trip order is associated with status $o = (u, v, \xi)$ if it originates from u , heads to v , and has been

²We can extend our model to account for non-linear charging rates, see our numerical experiment in Sec. 6.

waiting for vehicle assignment in the system for ξ time steps. A trip with origin u and destination v can be served by a vehicle of status (u, η, b) if (1) the vehicle can reach u within the passenger's pickup-patience time L_p (i.e. $\eta \leq L_p$), and (2) the remaining battery of the vehicle when reaching u is sufficient to complete the trip to v (i.e. $b \geq b_{uv}$). We note that a vehicle may be assigned to pick up a new passenger before completing its current trip towards u as long as it can arrive within L_p time steps. We use $\mathcal{O} := \{(u, v, \xi)\}_{u, v \in V, \xi=0, \dots, L_c}$ to denote the set of all trip status.

A charger is associated with status $w = (v, \delta, j)$ if it is located at region v with a rate of δ and is j time steps away from being available. Specifically, if $j = 0$, the charger is available immediately. If $j > 0$, the charger is currently in use and will take an additional j time steps to complete the charging period. We use $\mathcal{W} := \{(v, \delta, j)\}_{v \in V, \delta \in \Delta, j=0, \dots, J-1}$ to denote the set of all charger status. All notations introduced in this section are summarized in Table 1.

2.2 Markov decision process

We next describe the *state*, *action*, *policy* and *reward* of the Markov decision process (MDP).

State. We denote the state space of the MDP as \mathcal{S} with generic element s . The state vector $s^{t,d} = \left(t, \left(s_c^{t,d} \right)_{c \in \mathcal{C}}, \left(s_o^{t,d} \right)_{o \in \mathcal{O}}, \left(s_w^{t,d} \right)_{w \in \mathcal{W}} \right) \in \mathcal{S}$ records the fleet state $\left(s_c^{t,d} \right)_{c \in \mathcal{C}}$, the trip order state $\left(s_o^{t,d} \right)_{o \in \mathcal{O}}$, and the charger state $\left(s_w^{t,d} \right)_{w \in \mathcal{W}}$ for each time t of day d , where $s_c^{t,d}$ is the number of vehicles of status c , $s_o^{t,d}$ is the number of trip orders of status o , and $s_w^{t,d}$ is the number of chargers of status w at (t, d) . For all (t, d) , the sum of vehicles of all statuses equals to the fleet size N . That is,

$$\sum_{c \in \mathcal{C}} s_c^{t,d} = N, \quad \forall t \in [T], d = 1, 2, \dots \quad (1)$$

Additionally, the sum of chargers of all remaining charging times for each region v and rate δ equals to the quantity of the corresponding charging facility n_v^δ . That is, for all $v \in V$ and all $\delta \in \Delta$,

$$\sum_{j=0}^J s_{(v, \delta, j)}^{t,d} = n_v^\delta, \quad \forall t \in [T], d = 1, 2, \dots \quad (2)$$

Moreover, we note that while the number of new trip arrivals $X_{uv}^{t,d}$ can be unbounded, the maximum number of trip orders that can be served before abandonment at any time step is at most $N(L_c + 1)$. This is because the fleet can serve up to N trips per time step, and each trip order remains active for at most L_c steps before being abandoned. As a result, without loss of generality, we can upper bound $s_o^{t,d}$ for each status o by $N(L_c + 1)$, with any additional trip requests beyond this limit rejected by the system. Hence, our state space \mathcal{S} is finite.

Action. We denote the action space of the MDP as \mathcal{A} with generic element a . An action is a flow vector of the fleet that consists of the number of vehicles of each status assigned to take

trips, reposition, charge, and pass. We denote an action vector at time t of day d as $a^{t,d} := \left(f_c^{t,d}, e_c^{t,d}, q_c^{t,d}, p_c^{t,d} \right)_{c \in \mathcal{C}}$, where:

- $f_c^{t,d} := \left(f_{c,o}^{t,d} \in \mathbb{N} \right)_{o \in \mathcal{O}}$ determines the number of vehicles of each status c assigned to fulfill each trip order status $o \in \mathcal{O}$ at time t of day d . In particular, vehicles are eligible to take trip requests if their current location or destination matches the trip's origin region, they are within L_p time steps from completing the current task, and they have sufficient battery to complete the trip, i.e.

$$f_{c,o}^{t,d} \begin{cases} \geq 0, & \forall c = (u, \eta, b) \text{ and } o = (u, v, \xi) \\ & \text{such that } \eta \leq L_p \text{ and } b \geq b_{uv}, \\ = 0, & \text{otherwise.} \end{cases} \quad (3)$$

Additionally, we require that the total number of vehicles that fulfill the trip orders of status o cannot exceed $s_o^{t,d}$, i.e.

$$\sum_{c=(u,\eta,b) \in \mathcal{C}} f_{c,o}^{t,d} \leq s_o^{t,d}, \quad \forall o = (u, v, \xi) \in \mathcal{O}. \quad (4)$$

- $e_c^{t,d} := \left(e_{c,v}^{t,d} \in \mathbb{N} \right)_{v \in V}$ represents the number of vehicles of each status c assigned to reposition to v at time t of day d . In particular, vehicles are eligible to reposition to a different region if they have already completed their current tasks and they have sufficient battery to complete the trip.

$$e_{c,v}^{t,d} \begin{cases} \geq 0, & \forall c = (u, \eta, b) \text{ and } v \neq u \\ & \text{such that } \eta = 0 \text{ and } b \geq b_{uv}, \\ = 0, & \text{otherwise.} \end{cases} \quad (5)$$

- $q_c^{t,d} := \left(q_{c,\delta}^{t,d} \in \mathbb{N} \right)_{\delta \in \Delta}$ represents the number of vehicles of status c assigned to charge with rate δ at time t of day d . In particular, vehicles are eligible to charge if they are idling in the region where the charger is located:

$$q_{c,\delta}^{t,d} \begin{cases} \geq 0, & \forall c = (u, \eta, b) \text{ and } \delta \in \Delta \\ & \text{such that } \eta = 0, \\ = 0, & \text{otherwise.} \end{cases} \quad (6)$$

Additionally, for each region v and charging rate δ , we require that the total number of vehicles of all statuses assigned to charge at region v with rate δ cannot exceed the total number of available chargers:

$$\sum_{c=(v,\eta,b) \in \mathcal{C}} q_{c,\delta}^{t,d} \leq s_{(v,\delta,0)}^{t,d}, \quad \forall v \in V, \delta \in \Delta. \quad (7)$$

- $p_c^{t,d} \in \mathbb{N}$ represents the number of vehicles of status c not assigned with any new action at time t of day d . All vehicles are eligible for the pass action.

For any t and d , the vector $a^{t,d}$ needs to satisfy the following flow conservation constraint: All vehicles of each status should be assigned to one of the trip-fulfilling, repositioning, charging, or passing actions. That is,

$$\sum_{o \in \mathcal{O}} f_{c,o}^{t,d} + \sum_{v \in V} e_{c,v}^{t,d} + \sum_{\delta \in \Delta} q_{c,\delta}^{t,d} + p_c^{t,d} = s_c^{t,d},$$

$$\forall c \in \mathcal{C}, t \in [T], d = 1, 2, \dots \quad (8)$$

From the above description, we note that the feasibility of an action depends on the state. We denote the set of actions that are feasible for state s as \mathcal{A}_s .

Policy. The policy $\pi : \mathcal{S} \rightarrow \Delta(\mathcal{A}_s)$ is a randomized policy that maps the state vector to an action, where $\pi(a|s)$ is the probability of choosing action a given state s under policy π . We note that the notation $\pi(\cdot)$ does not explicitly depend on t because t is already included as a part of the state vector s .

State Transitions. At any time t of day d , given any state s and action $a \in \mathcal{A}_s$, we compute the vehicle state vector at time $t + 1$. For each vehicle status $c := (v, \eta, b) \in \mathcal{C}$,

$$s_{(v,\eta,b)}^{t+1,d} = \left(\sum_{u \in V} \sum_{c'=(u,\eta',b') \in \mathcal{C}} \sum_{o=(u,v,\xi') \in \mathcal{O}} f_{c',o}^{t,d} \mathbb{1}(\eta' + \tau_{uv}^t - 1 = \eta, b' - b_{uv} = b) \right) \quad (i)$$

$$+ \left(\sum_{u \in V} \sum_{c'=(u,0,b') \in \mathcal{C}} e_{c',v}^{t,d} \cdot \mathbb{1}(\tau_{uv}^t - 1 = \eta, b' - b_{uv} = b) \right) \quad (ii)$$

$$+ \left[\left(\sum_{\delta \in \Delta} q_{(v,0,b-\delta J),\delta}^{t,d} \mathbb{1}(\eta = J-1, b \geq \delta J) \right) + \left(\sum_{b' > b - \delta J} \sum_{\delta \in \Delta} q_{(v,0,b'),\delta}^{t,d} \mathbb{1}(\eta = J-1, b = B) \right) \right] \quad (iii)$$

$$+ \underbrace{p_{(v,\eta,b)}^{t,d} \mathbb{1}(\eta = 0)}_{(iv)} + \underbrace{p_{(v,\eta+1,b)}^{t,d} \mathbb{1}(\eta > 0)}_{(v)}, \quad (9)$$

where (i) and (ii) correspond to vehicles assigned to new trip-fulfilling or repositioning actions with destination v , respectively. The destination, time to arrival, and battery level of these vehicles are updated based on the newly assigned trips. Term (iii) corresponds to the vehicles assigned to charge at time t . The battery level of these vehicles will be increased by δJ at the end of the charging

period. If the vehicle is charged to full, then it will remain idle for the rest of the charging period. Term (iv) corresponds to the idling vehicles that continue to remain idle, and (v) corresponds to the vehicles taking the passing action whose remaining time of completing the current action decreases by 1 in the next time step.

Moreover, the trip state at time $t + 1$ of day d is given by (10). For each trip status, we subtract the number of trip orders that have been fulfilled at time t , and we increment the active time by 1 for trip orders that are still in the system. We abandon the trip orders that have been active for more than L_c time steps. Additionally, new trip orders arrive in the system and we set their active time in the system to be 0. That is, for all $(u, v) \in V \times V$,

$$s_{(u,v,\xi)}^{t+1,d} = \begin{cases} \min \left\{ X_{uv}^{t,d}, N(L_c + 1) \right\}, & \text{if } \xi = 0, \\ s_{(u,v,\xi-1)}^{t,d} - \sum_{c \in \mathcal{C}} f_{c,(u,v,\xi-1)}^{t,d}, & \text{if } 1 \leq \xi \leq L_c. \end{cases} \quad (10)$$

As mentioned earlier in this section, we cap the number of new trip arrivals by $N(L_c + 1)$ so that the state space is finite. Then, trips that are not fulfilled at time t are queued to $t + 1$. Thus, the number of trips that have been in the system for $\xi \geq 1$ at time $t + 1$ equals to that with $\xi - 1$ from time t minus the ones that are assigned to a vehicle at time t .

Lastly, the charger state at time $t + 1$ of day d is given by (11). For each charger status $w := (v, \delta, j) \in \mathcal{W}$: For all region $v \in V$ and for all charger outlet rates $\delta \in \Delta$,

$$s_{(v,\delta,j)}^{t+1,d} = \begin{cases} \sum_{c=(v,0,b) \in \mathcal{C}} q_{c,\delta}^{t,d}, & \text{if } j = J - 1, \\ s_{(v,\delta,j+1)}^{t,d}, & \text{if } 0 < j < J - 1, \\ s_{(v,\delta,1)}^{t,d} + \left(s_{(v,\delta,0)}^{t,d} - \sum_{c=(v,0,b) \in \mathcal{C}} q_{c,\delta}^{t,d} \right), & \text{if } j = 0. \end{cases} \quad (11)$$

At time $t + 1$, the number of chargers that are occupied with remaining time $j = J - 1$ equals the total number of vehicles just assigned to charge at time t . Chargers already in use at time t will have their remaining charging time j decrease by 1 when the system transitions to time $t + 1$. The number of chargers available (i.e. $j = 0$) at time $t + 1$ consists of (i) the chargers that have just completed their charging periods (i.e. $s_{(v,\delta,1)}^{t,d}$), and (ii) the chargers available at time t minus the ones that are assigned to charge vehicles (i.e. $s_{(v,\delta,0)}^{t,d} - \sum_{c=(v,0,b) \in \mathcal{C}} q_{c,\delta}^{t,d}$).

Reward. The reward of fulfilling a trip request from u to v at time t is $r_{f,uv}^t \in \mathbb{R}_{\geq 0}$. We remark that if a trip request has been active in the system for some time, then the reward is determined by the time at which the trip request is picked up. The reward (cost) of re-routing between u, v is $r_{e,uv}^t \in \mathbb{R}_{\leq 0}$. The reward (cost) for a vehicle to charge at time t is $r_{q,\delta}^t \in \mathbb{R}_{\leq 0}$. Idling and passing actions incur no reward or cost. As a result, given the action $a^{t,d}$, the total reward at time t of day

d is given by

$$\begin{aligned} r^t(a^{t,d}) &= \sum_{c \in \mathcal{C}} \sum_{(u,v) \in V \times V} \sum_{\xi=0}^{L_c} r_{f,uv}^t f_{c,(u,v,\xi)}^{t,d} \\ &+ \sum_{c \in \mathcal{C}} \sum_{(u,v) \in V \times V} r_{e,uv}^t e_{c,v}^{t,d} + \sum_{c \in \mathcal{C}} \sum_{\delta \in \Delta} r_{q,\delta}^t q_{c,\delta}^{t,d}. \end{aligned} \quad (12)$$

The long-run average daily reward of a policy π given some initial state s is as follows:

$$R(\pi|s) := \lim_{D \rightarrow \infty} \frac{1}{D} \mathbb{E}_\pi \left[\sum_{d=1}^D \sum_{t=1}^T r^t(a^{t,d}) \mid s \right]. \quad (13)$$

Since the state is finite and the state transition and policy are homogeneous across days, the limit defined above exists (see page 337 of [91]). Our goal is to find the optimal fleet control policy π^* that maximizes the long-run average daily rewards given *any* initial state s :

$$R^*(s) = R(\pi^*|s) = \max_{\pi} R(\pi|s), \quad \forall s \in \mathcal{S}. \quad (14)$$

3 Fleet Control Policy Reduction With Atomic Actions

One challenge of computing the optimal control policy lies in the size of the action space $|\mathcal{A}|$, which grows exponentially with the number of vehicles N and vehicle statuses $|\mathcal{C}|$. As a result, the dimension of policy π also grows exponentially with N and $|\mathcal{C}|$. The focus of this section is to address this challenge by introducing a policy reduction scheme, which decomposes fleet dispatching to sequential assignment of tasks to individual vehicles, where the task for each individual vehicle is referred as an “atomic action”. We use the name “atomic action policy” because each atomic action only changes the status of a single vehicle. In particular, for any vehicle of a status $c \in \mathcal{C}$, an atomic action can be any one of the followings:

- \hat{f}_o represents fulfilling a trip of status $o \in \mathcal{O}$.
- \hat{e}_v represents repositioning to destination $v \in V$.
- \hat{q}_δ represents charging with rate $\delta \in \Delta$ at its current region.
- \hat{p} represents continuing with its previously assigned actions.

We use $\hat{\mathcal{A}}$ to denote the atomic action space that includes all of the above atomic actions, i.e. $\hat{a} \in \hat{\mathcal{A}} := \left\{ \left(\hat{f}_o \right)_{o \in \mathcal{O}}, (\hat{e}_v)_{v \in V}, (\hat{q}_\delta)_{\delta \in \Delta}, \hat{p} \right\}$. The atomic action significantly reduces the dimension of the action function since $\hat{\mathcal{A}}$ does not scale with the fleet size or the number of vehicle statuses.

We now present the procedure of atomic action assignment. In each decision epoch (t, d) , vehicles are arbitrarily indexed from 1 to N , and are sequentially selected. For a selected vehicle

Symbol	Description
V	The set of all service regions
N	Fleet Size
B	Vehicle battery range
Δ	Set of charging rates
T	Number of time steps of each single day
τ_{uv}^t	Trip duration from u to v at time t
b_{uv}	Battery consumption for traveling from region u to v
n_v^δ	Number of chargers of rate δ at region v
λ_{uv}^t	Trip arrival rate from u to v at time t
$X_{uv}^{t,d}$	Number of trip requests from u to v at time t of day d
L_p	Maximum pickup patience time
L_c	Maximum assignment patience time
J	Duration of a charging period
\mathcal{C}	The set of all vehicle statuses, with a generic vehicle status denoted as c
\mathcal{O}	The set of all trip statuses, with a generic trip status denoted as o
\mathcal{W}	The set of all charger statuses, with a generic charger status denoted as w
$s^{t,d}$	The state vector at time t of day d
$a^{t,d}$	The fleet action vector at time t of day d
$f_{c,o}^{t,d}$	The number of vehicles of status c assigned to fulfill trips of status o at time t of day d
$e_{c,v}^{t,d}$	The number of vehicles of status c assigned to reposition to region v at time t of day d
$q_{c,\delta}^{t,d}$	The number of vehicles of status c assigned to charge with rate δ at time t of day d
$p_c^{t,d}$	The number of vehicles of status c assigned to pass at time t of day d
$r^t(a)$	The reward given action a at time t

Table 1: Notations for the electric robo-taxi system.

n , the atomic policy $\hat{\pi} : \mathcal{S} \times \mathcal{C} \rightarrow \Delta(\hat{\mathcal{A}})$ maps from the tuple of system state $s_n^{t,d}$ before the n -th assignment and the selected vehicle's status c_n to a distribution of atomic actions. The system state $s_n^{t,d}$ updates after each individual vehicle assignment, starting with $s_1^{t,d} = s^{t,d}$. After the final vehicle is assigned and the new trip arrivals at time $t+1$ are realized, the state $s_N^{t,d}$ transitions to $s^{t+1,d}$.

The total reward for each decision epoch (t, d) is the sum of all rewards generated from each atomic action assignment in (t, d) , where the reward generated by the atomic action $\hat{a}^{t,d} \in \hat{\mathcal{A}}$ on a

vehicle of status $c^{t,d} := (u, \eta, b) \in \mathcal{C}$ is given by

$$\begin{aligned} r^t(c^{t,d}, \hat{a}^{t,d}) &= \sum_{o \in \mathcal{O}} r_{f,o}^t \mathbb{1} \left\{ \hat{a}^{t,d} = \hat{f}_o \right\} \\ &+ \sum_{(u,v) \in V \times V} r_{e,uv}^t \mathbb{1} \left\{ \hat{a}^{t,d} = \hat{e}_v \right\} \\ &+ \sum_{\delta \in \Delta} r_{q,\delta}^t \mathbb{1} \left\{ \hat{a}^{t,d} = \hat{q}_\delta \right\}. \end{aligned}$$

The long-run average reward given the atomic action policy $\hat{\pi}$ and the initial state $s \in \mathcal{S}$ is as follows:

$$\begin{aligned} R(\hat{\pi}|s) &= \lim_{D \rightarrow \infty} \frac{1}{D} \mathbb{E}_{\hat{\pi}} \left[\sum_{d=1}^D \sum_{t=1}^T \sum_{n=1}^N r^t(c_n^{t,d}, \hat{a}_n^{t,d}) \middle| s \right], \\ &\forall s \in \mathcal{S}, \end{aligned}$$

where $\hat{a}_n^{t,d}$ is the atomic action generated by the atomic action policy and $c_n^{t,d}$ is the status of vehicle to be assigned in the n -th atomic step in decision epoch (t, d) . Given any initial state $s \in \mathcal{S}$, the optimal atomic action policy is given by $\hat{\pi}^* = \text{argmax}_{\hat{\pi}} R(\hat{\pi}|s)$.

Our atomic action policy can be viewed as a reduction of the original fleet dispatching policy in that any realized sequence of atomic actions corresponds to a feasible fleet dispatching action with the same reward of the decision epoch. This reduction makes the training of atomic action policy scalable because the output dimension of atomic action policy $\hat{\pi}^t$ equals to $|\hat{\mathcal{A}}|$, which is a constant regardless of the fleet size.

4 Deep Reinforcement Learning With Aggregated States

The adoption of atomic actions has significantly reduced the action dimension. However, computing the optimal atomic action policy is still challenging due to the large state space, which scales significantly with the fleet size, number of regions, and battery discretization. In this section, we provide an efficient algorithm to train the fleet dispatching policy by incorporating our atomic action decomposition into the Proximal Policy Optimization (PPO) framework [2]. To tackle with the large state size, we use neural networks to approximate both the value function and the policy function, to be specified later. We also further reduce the state size using the following state reduction scheme:

Battery Level Clustering. We map the state representation of all vehicle statuses into vehicle statuses with aggregated battery levels. We cluster the battery levels into 3 intervals, each of which denotes low battery level b_L , medium battery level b_M , and high battery level b_H , respectively. The cutoff points can be set based on charging rates and criticality of battery levels. It is also possible

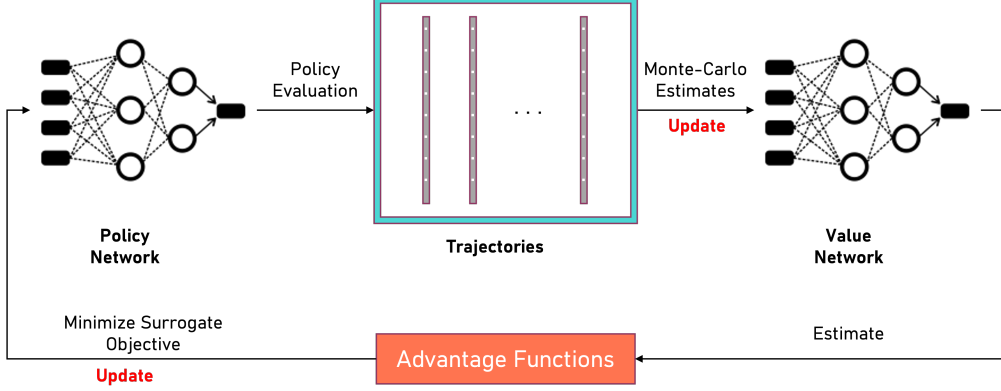


Figure 1: Atomic-PPO Training Pipeline

to cluster the battery levels differently. If computing resources allow, we can cluster the battery levels with finer granularity, e.g. into 10 levels instead of 3.

Trip Order Status Clustering. In the state reduction scheme, trip orders are aggregated by recording only the number of requests originating from or arriving at each region, instead of tracking the number of trip requests for each origin-destination pair. The clustering of trip order statuses reduces the state dimension from $O(|V|^2)$ to $O(|V|)$. While it loses some information about the trip distribution, in numerical experiments, we demonstrate that the vehicle dispatching policy trained using our state reduction scheme still achieves a very strong performance (see Section 6).

We denote the state space after the reduction on the original state as $\bar{\mathcal{S}}$, which we refer to as the “reduced state space”. We use neural network $\hat{\pi}_\theta : \bar{\mathcal{S}} \times \mathcal{C} \rightarrow \Delta(\hat{\mathcal{A}})$ on the reduced state space to approximate the atomic action policy function, where θ is the parameter vector for the atomic policy network. Our Atomic-PPO algorithm (Figure 1) is formally presented in Algorithm 1. For each policy iteration $m = 1, \dots, M$, we maintain a copy of the policy neural network parameters θ_{m-1} from the previous iteration and keep it fixed throughout the iteration. We then generate a dataset $\text{Data}_{\theta_{m-1}}^{(K)}$ by simulating K trajectories given the atomic action policy $\hat{\pi}_{\theta_{m-1}}$. For each decision epoch (t, d) and each trajectory k , this dataset includes the reduced state $\bar{s}_n^{t,d,(k)}$, the status $c_n^{t,d,(k)}$ of vehicle to be assigned, atomic action $\hat{a}_n^{t,d,(k)}$, and atomic reward $r^t(c_n^{t,d,(k)}, \hat{a}_n^{t,d,(k)})$ for each atomic step with $n = 1, \dots, N$. That is,

$$\begin{aligned} \text{Data}_{\theta_{m-1}}^{(K)} := & \left\{ \left[\left[\left(\bar{s}_n^{t,d,(k)}, c_n^{t,d,(k)}, \hat{a}_n^{t,d,(k)}, \right. \right. \right. \right. \right. \\ & \left. \left. \left. \left. \left. \left. r^t(c_n^{t,d,(k)}, \hat{a}_n^{t,d,(k)}) \right)^N \right]^T \right]^D \right\}_{k=1}^K. \end{aligned} \quad (15)$$

In each trajectory, we truncate the roll-out to D days, with T time steps in each day. Here, we set D to be number that is large enough so that the distribution of the system state on day D is close

Algorithm 1: The Atomic-PPO Algorithm

Inputs: Number of policy iterations M , number of trajectories per policy iteration K , number of days per trajectory D , initial policy network $\hat{\pi}_{\theta_0}$.

for *policy iteration* $m = 1, \dots, M$ **do**

Run policy $\hat{\pi}_{\theta_{m-1}}$ over K Monte Carlo trajectories, each spanning D days and T time steps per day. Collect the dataset as in (15).

Compute empirical estimate of the long-run average daily reward (16).

Compute empirical estimates of the relative value function (18).

Update relative value network by minimizing the mean-squared error (19).

Estimate advantage functions as in (20).

Obtain the updated policy network $\hat{\pi}_{\theta_m}$ by maximizing the surrogate objective function (21).

end

return *policy* $\hat{\pi}_{\theta_M}$

to the stationary state distribution regardless of the initial state. The procedure for the sequential assignment of atomic actions to individual vehicles follows from Section 3. Using the collected data, we estimate:

(i) The long-run average daily reward $g_{\theta_{m-1}} := R(\hat{\pi}_{\theta_{m-1}})$ for policy $\hat{\pi}_{\theta_{m-1}}$ ³:

$$\hat{g}_{\theta_{m-1}} = \frac{1}{KD} \sum_{k=1}^K \sum_{d=1}^D \sum_{t=1}^T \sum_{n=1}^N r^t(c_n^{t,d,(k)}, \hat{a}_n^{t,d,(k)}), \quad (16)$$

where we use $\hat{g}_{\theta_{m-1}}$ to denote the empirical estimate of long-run average daily reward of $\hat{\pi}_{\theta_{m-1}}$.

(ii) The relative value function $h_{n,\theta_{m-1}} : \mathbb{R}^{|\mathcal{S}|} \rightarrow \mathbb{R}$ given policy $\hat{\pi}_{\theta_{m-1}}$ for each atomic step $n \in [N]$:

The relative value function quantifies how much better (or worse) each state is relative to the average. In particular, for any state $s \in \mathcal{S}$, where we recall that s contains the time of day t information,

³For simplicity, we present the algorithm under the assumption that the system has a single recurrent class, so the long-run average reward does not depend on the initial system state. Our approach can generalize to multi-chain systems.

we define its relative value $h_{n,\theta_{m-1}}(s)$ under policy $\hat{\pi}_{\theta_{m-1}}$ at atomic step $n \in [N]$ as:

$$\begin{aligned}
& h_{n,\theta_{m-1}}(s) \\
&= \mathbb{E}_{\hat{\pi}_{\theta_{m-1}}} \left[\sum_{i=n}^N \left(r^t(c_i^{t,1}, \hat{a}_i^{t,1}) - \frac{1}{TN} g_{\theta_{m-1}} \right) \right. \\
&\quad + \sum_{\ell=t+1}^T \sum_{i=1}^N \left(r^\ell(c_i^{\ell,1}, \hat{a}_i^{\ell,1}) - \frac{1}{TN} g_{\theta_{m-1}} \right) \\
&\quad \left. \left| s_n^{t,1} = s \right. \right] \\
&\quad + \sum_{d=2}^{\infty} \sum_{\ell=1}^T \sum_{i=1}^N \\
&\quad \mathbb{E}_{\hat{\pi}_{\theta_{m-1}}} \left[\left(r^\ell(c_i^{\ell,d}, \hat{a}_i^{\ell,d}) - \frac{1}{TN} g_{\theta_{m-1}} \right) \right. \\
&\quad \left. \left| s_n^{t,1} = s \right. \right], \quad \forall s \in \mathcal{S}, \forall t \in [T]. \tag{17}
\end{aligned}$$

Remark 1. By Proposition 2 in our concurrent work [92], the infinite series in (17) is well defined. Additionally, under the atomic action decomposition, the Markov chain has a period of TN , which is the total number of atomic steps in each day. The definition of the relative value function is equivalent to the one defined using the Cesaro limit, as given by Puterman (see page 338 of [91]) for periodic chains, up to an additive constant (see Proposition 3 in [92]).

For any state $s_n^{t,d,(k)}$ in the atomic step n of trajectory k of decision epoch (t, d) , we construct an empirical estimate $\hat{h}_{n,\theta_{m-1}}^{t,d,(k)}$ of its relative value function $h_{n,\theta_{m-1}}(s_n^{t,d,(k)})$ as:

$$\begin{aligned}
& \hat{h}_{n,\theta_{m-1}}^{t,d,(k)} \\
&:= \sum_{i=n}^N \left(r^t(c_i^{t,d,(k)}, \hat{a}_i^{t,d,(k)}) - \frac{1}{TN} \hat{g}_{\theta_{m-1}} \right) \\
&\quad + \sum_{\ell=t+1}^T \sum_{i=1}^N \left(r^\ell(c_i^{\ell,d,(k)}, \hat{a}_i^{\ell,d,(k)}) - \frac{1}{TN} \hat{g}_{\theta_{m-1}} \right) \\
&\quad + \sum_{d'=d+1}^D \sum_{\ell=1}^T \sum_{i=1}^N \left(r^\ell(c_i^{\ell,d',(k)}, \hat{a}_i^{\ell,d',(k)}) - \frac{1}{TN} \hat{g}_{\theta_{m-1}} \right). \tag{18}
\end{aligned}$$

Due to the large state space, we cluster the state into reduced states as described in earlier parts of Section 4. Then, we use neural networks $h_{\psi_{m-1}} : \bar{\mathcal{S}} \rightarrow \mathbb{R}$ on the reduced state space to approximate the relative value function for all atomic steps, where ψ_{m-1} is the network parameters. We learn $h_{\psi_{m-1}}$ by minimizing the mean-square loss given the empirical estimates:

$$\sum_{k=1}^K \sum_{d=1}^D \sum_{t=1}^T \sum_{n=1}^N \left(h_{\psi_{m-1}}(\bar{s}_n^{t,d,(k)}) - \hat{h}_{n,\theta_{m-1}}^{t,d,(k)} \right)^2. \tag{19}$$

(iii) The advantage function of $\hat{\pi}_{\theta_{m-1}}$:

The advantage function quantifies the change in the long-run average reward resulting from deviating from the previous stage policy $\hat{\pi}_{\theta_{m-1}}$ by selecting the atomic action $\hat{a}_n^{t,d,(k)}$ at a given state $s_n^{t,d,(k)}$. The empirical estimates of the advantage function is given by:

$$\hat{A}_{\theta_{m-1}}(\bar{s}_n^{t,d,(k)}, c_n^{t,d,(k)}, \hat{a}_n^{t,d,(k)}) := \begin{cases} r^t(c_n^{t,d,(k)}, \hat{a}_n^{t,d,(k)}) - \frac{1}{TN} \hat{g}_{\theta_{m-1}} + \\ h_{\psi_{m-1}}(\bar{s}_{n+1}^{t,d,(k)}) - h_{\psi_{m-1}}(\bar{s}_n^{t,d,(k)}), \\ \quad \text{for all } n < N, \\ r^t(c_n^{t,d,(k)}, \hat{a}_n^{t,d,(k)}) - \frac{1}{TN} \hat{g}_{\theta_{m-1}} + \\ h_{\psi_{m-1}}(\bar{s}_1^{t+1,d,(k)}) - h_{\psi_{m-1}}(\bar{s}_n^{t,d,(k)}), \\ \quad \text{if } n = N, t < T, \\ r^t(c_n^{t,d,(k)}, \hat{a}_n^{t,d,(k)}) - \frac{1}{TN} \hat{g}_{\theta_{m-1}} + \\ h_{\psi_{m-1}}(\bar{s}_1^{1,d+1,(k)}) - h_{\psi_{m-1}}(\bar{s}_n^{t,d,(k)}), \\ \quad \text{if } n = N, t = T. \end{cases} \quad (20)$$

Using the estimated advantage function $\hat{A}_{\theta_{m-1}}$, the Atomic-PPO algorithm computes the atomic action policy function of the next iteration $\hat{\pi}_{\theta_m}$ by choosing parameter θ_m that maximizes the clipped surrogate function defined as follows:

$$\begin{aligned} \hat{L}(\theta_m, \theta_{m-1}) &:= \frac{1}{K} \sum_{k=1}^K \sum_{d=1}^D \sum_{t=1}^T \sum_{n=1}^N \\ &\min \left(\frac{\hat{\pi}_{\theta_m}(\hat{a}_n^{t,d,(k)} | \bar{s}_n^{t,d,(k)}, c_n^{t,d,(k)})}{\hat{\pi}_{\theta_{m-1}}(\hat{a}_n^{t,d,(k)} | \bar{s}_n^{t,d,(k)}, c_n^{t,d,(k)})} \cdot \right. \\ &\hat{A}_{\theta_{m-1}}(\bar{s}_n^{t,d,(k)}, c_n^{t,d,(k)}, \hat{a}_n^{t,d,(k)}), \\ &\left. \text{clip} \left(\frac{\hat{\pi}_{\theta_m}(\hat{a}_n^{t,d,(k)} | \bar{s}_n^{t,d,(k)}, c_n^{t,d,(k)})}{\hat{\pi}_{\theta_{m-1}}(\hat{a}_n^{t,d,(k)} | \bar{s}_n^{t,d,(k)}, c_n^{t,d,(k)})}, 1 - \epsilon, 1 + \epsilon \right) \cdot \right. \\ &\left. \hat{A}_{\theta_{m-1}}(\bar{s}_n^{t,d,(k)}, c_n^{t,d,(k)}, \hat{a}_n^{t,d,(k)}) \right), \end{aligned} \quad (21)$$

where $\epsilon > 0$ is a hyperparameter referred as the clip size of the training. The policy update builds on the original PPO that is known for its training stability by performing conservative policy updates. Specifically, the update uses the clipped surrogate function (21) to limit the change in the policy by bounding the ratio between the new and old policy probabilities within a clip range defined by ϵ .

5 Reward Upper Bound Provided By Fluid Approximation Model

Before presenting the performance of our atomic PPO algorithm, we construct an upper bound on the optimal long-run average reward using fluid limit. This upper bound will be used to assess the performance of our atomic PPO algorithm in numerical experiments as shown in the next section. We formulate a fluid-based linear optimization program, where the fluid limit is attained as the fleet size approaches infinity, with both trip arriving rates and charger numbers scaling up proportionally to the fleet size. Under the fluid limit, the system becomes deterministic, and the fleet dispatching policy, which is a probability distribution of vehicle flows across all actions, reduces to a deterministic vector that represents the fraction of fleet assigned to each action at each time of the day. We define the decision variables of the fluid-based optimization problem as follows:

- *Fraction of fleet for trip fulfilling* $\bar{f} := (\bar{f}_{c,o}^t)_{c \in \mathcal{C}, o \in \mathcal{O}, t \in [T]}$, where $\bar{f}_{c,o}^t$ is the fraction of vehicles with status c fulfilling trip requests of status o at time t .
- *Fraction of fleet for repositioning* $\bar{e} := (\bar{e}_{c,v}^t)_{c \in \mathcal{C}, v \in \mathcal{V}, t \in [T]}$, where $\bar{e}_{c,v}^t$ is the fraction of vehicles with status c repositioning to v at time t .
- *Fraction of fleet for charging* $\bar{q} := (\bar{q}_{c,\delta}^t)_{c \in \mathcal{C}, \delta \in \Delta, t \in [T]}$, where $\bar{q}_{c,\delta}^t$ is the fraction of vehicles with status c charging with rate δ at time t .
- *Fraction of fleet for continuing the current action* $\bar{p} := (\bar{p}_c^t)_{c \in \mathcal{C}, t \in [T]}$, where \bar{p}_c^t is the fraction of fleet with status c taking the passing action at time t .

The fluid-based linear program aims at maximizing the total reward achieved by the fluid policy:

$$\begin{aligned} \max_{\bar{f}, \bar{e}, \bar{q}, \bar{p}} \quad & N \sum_{t \in [T]} \sum_{c \in \mathcal{C}} \left[\sum_{u \in \mathcal{V}} \sum_{v \in \mathcal{V}} \left[r_{f,uv}^t \left(\sum_{\xi \in [L_c]} \bar{f}_{c,(u,v,\xi)}^t \right) \right. \right. \\ & \left. \left. + r_{e,uv}^t \bar{e}_{c,v}^t \right] + \sum_{\delta \in \Delta} r_{q,\delta}^t \bar{q}_{c,\delta}^t \right], \end{aligned} \quad (\text{Fluid-LP})$$

s.t. Constraints (22) – (28).

The constraints (22)-(28) are given as follows:

1. The flow conservation for each vehicle status $c := (v, \eta, b) \in \mathcal{C}$ at each time t of a day.
In particular, the left-hand side of constraint (22) represents the fraction of fleet that transitions to vehicle status c according to (9) at time t . The right-hand side of constraint (22) represents the total fraction of fleet with status c that is assigned to trip-fulfilling, reposition-

ing, charging, and passing actions.

$$\begin{aligned}
& \left(\sum_{u \in V} \sum_{c'=(u,\eta',b') \in \mathcal{C}} \sum_{o=(u,v,\xi') \in \mathcal{O}} \right. \\
& \quad \left. \bar{f}_{c',o}^{t-1} \mathbb{1}(\eta' + \tau_{uv}^{t-1} - 1 = \eta, b' - b_{uv} = b) \right) \\
& \quad + \left(\sum_{u \in V} \sum_{c'=(u,0,b') \in \mathcal{C}} \bar{e}_{c',v}^{t-1} \cdot \right. \\
& \quad \left. \mathbb{1}(\tau_{uv}^{t-1} - 1 = \eta, b' - b_{uv} = b) \right) \\
& \quad + \left[\left(\sum_{\delta \in \Delta} \bar{q}_{(v,0,b-\delta J),\delta}^{t-1} \mathbb{1}(\eta = J-1, b \geq \delta J) \right) + \right. \\
& \quad \left. \left(\sum_{b' > b-\delta J} \sum_{\delta \in \Delta} \bar{q}_{(v,0,b'),\delta}^{t-1} \mathbb{1}(\eta = J-1, b = B) \right) \right] \\
& \quad + \bar{p}_{(v,\eta,b)}^{t-1} \mathbb{1}(\eta = 0) + \bar{p}_{(v,\eta+1,b)}^{t-1} \mathbb{1}(\eta < \hat{\tau}) \\
& = \sum_{o \in \mathcal{O}} \bar{f}_{c,o}^t + \sum_{v \in V} \bar{e}_{c,v}^t + \sum_{\delta \in \Delta} \bar{q}_{c,\delta}^t + \bar{p}_c^t, \\
& \quad \forall c := (v, \eta, b) \in \mathcal{C}, \quad t \in [T], \tag{22}
\end{aligned}$$

We note that the time steps are periodic across days, and thus for $t = 1$ in (22), $t - 1$ is the last time step T of the previous day. Similarly, in all of the subsequent constraints (23) – (24), the time step t on the superscript of a variable being negative indicates time step $T - t$ of the previous day and $t > T$ indicates time step $t - T$ of the next day.

2. Trip order fulfillment does not exceed trip order arrivals:

$$\begin{aligned}
& \sum_{c=(u,\eta,b) \in \mathcal{C}} \sum_{o=(u,v,\xi) \in \mathcal{O}} \bar{f}_{c,o}^{t+\xi} \leq \frac{1}{N} \lambda_{uv}^t, \\
& \quad \forall u, v \in V, \quad t \in [T]. \tag{23}
\end{aligned}$$

3. The flow of charging vehicles in any region does not exceed the charger capacity.

$$\sum_{j \in [J]} \sum_{c=(v,0,b) \in \mathcal{C}} \bar{q}_{c,\delta}^{t-j} \leq \frac{1}{N} n_v^\delta, \quad \forall \delta \in \Delta, \quad t \in [T]. \tag{24}$$

4. Vehicles have sufficient battery to fulfill trips:

$$\begin{aligned}
& \bar{f}_{c,o}^t \mathbb{1}\{b < b_{uv}\} = 0, \\
& \quad \forall c = (u, \eta, b) \in \mathcal{C}, \quad o = (u, v, \xi) \in \mathcal{O}, \quad t \in [T]. \tag{25}
\end{aligned}$$

5. Vehicles have sufficient battery to reposition:

$$\begin{aligned}
& \bar{e}_{c,v}^t \mathbb{1}\{b < b_{uv}\} = 0, \\
& \quad \forall c = (u, \eta, b) \in \mathcal{C}, \quad v \in V, \quad t \in [T]. \tag{26}
\end{aligned}$$

6. The fractions of fleet of all statuses sum up to 1 at all time steps:

$$\sum_{c \in \mathcal{C}} \left[\sum_{o \in \mathcal{O}} \bar{f}_{c,o}^t + \sum_{v \in \mathcal{V}} \bar{e}_{c,v}^t + \sum_{\delta \in \Delta} \bar{q}_{c,\delta}^t + \bar{p}_c^t \right] = 1, \quad \forall t \in [T]. \quad (27)$$

7. All variables are non-negative.

$$\bar{f}, \bar{e}, \bar{q}, \bar{p} \geq 0. \quad (28)$$

Let \bar{R} be the optimal objective value of (Fluid-LP).

Theorem 1. $R^*(s) \leq \bar{R}, \quad \forall s \in \mathcal{S}$.

The proof of Theorem 1 is deferred to the Appendix. Theorem 1 shows that \bar{R} is an upper bound on the long-run average daily reward that can be achieved by any feasible policy. In the numerical section, we assess the ratio between the average daily reward achieved by our Atomic-PPO and the fluid upper bound \bar{R} . This ratio is a lower bound of the optimality ratio achieved by Atomic-PPO algorithm. We note that the current fluid-based linear program has $|V|(L_p + \hat{\tau})BT$ number of variables, where $\hat{\tau}$ can be large. In Appendix C, we present a reduction of (Fluid-LP) to reduce the number of variables to $|V|L_p BT$ without loss of optimality. This reduction leverages the fact that only vehicles with task remaining time $\eta \leq L_p$ can be assigned with new tasks, and therefore we only need to keep track of the fraction of fleet with statuses that are feasible for assigning new tasks.

6 Numerical Experiments

We conduct numerical experiments using the for-hire vehicle trip record data from July 2022, obtained from New York City Taxi and Limousine Commission’s (TLC) [8]. The dataset contains individual trip records of for-hire vehicles from Uber, Lyft, Yellow Cab, and Green Cab. Each trip record includes the origin and destination taxi zones, base passenger fares, trip duration, and distance, all of which are used for model calibration.

We consider trip requests from 0:00 to 24:00, Mondays to Thursdays ⁴, where each workday is partitioned into time intervals of 5 minutes. We estimate the arrival rate λ_{uv}^t for each origin u and destination v pair at each time t of a workday by averaging the number of trip requests from u to v at time t . Ride-hailing trips in NYC exhibit significant demand imbalances during the morning (7–10 am) and evening (5–8 pm) rush hours. As shown in Figure 2, certain zones experience more inbound trips (highlighted in red), while others see more outbound trips (in blue).

⁴We find that trip demand from Monday to Thursday follows a similar pattern, which differs from the patterns observed on Fridays through Sundays. Therefore, we use only the trip records from Monday to Thursday to calibrate the model for weekdays.

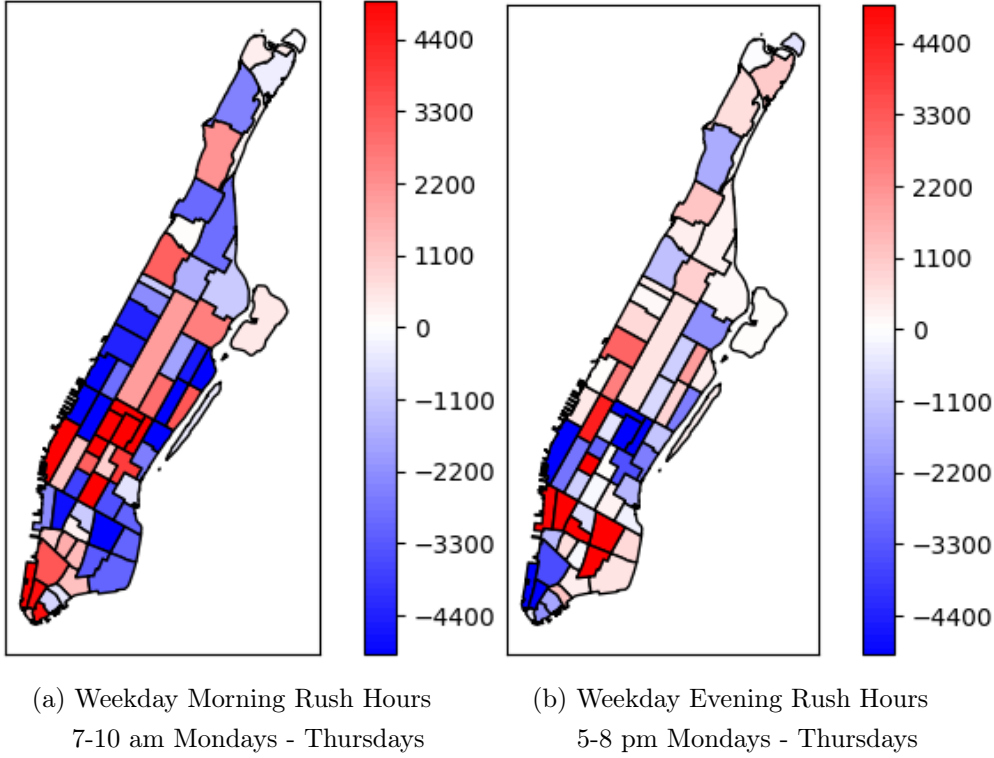


Figure 2: Manhattan Trip Demand Imbalance.

We partition the entire Manhattan into 10 regions (Figure 3) by aggregating adjacent taxi zones with similar demand patterns in both morning and evening rush hours. Based on trip request pattern, we identify 3 categories of regions: workplaces, restaurant areas, and residential areas. Workplaces are marked with red circles and mainly consist of downtown Manhattan and midtown Manhattan. Restaurants are mostly gathered in East Village and West Village circled in orange. Residential area consists of Upper/Midtown East, Upper/Midtown West, and upper Manhattan, and are circled in blue. During morning rush hours, people travel to workplaces (Figure 2a), while in the evening rush hours, they head to restaurants or residential areas (Figure 2b). Without repositioning, vehicles tend to idle in regions where inflow exceeds outflow, while trip requests are abandoned in regions where outflow exceeds inflow. Therefore, incorporating vehicle repositioning is critical for balancing supply across regions in Manhattan.

Using the NYC TLC dataset, we build a simulator of trip order arrival. We set the environment parameter for numerical experiments according to Table 2. The reward of a trip $r_{f,uv}^t$ from region u to v at time t is calibrated by taking the average of the base_passenger_fare column across all trips from u to v at time t . We estimate the actual fleet size using the maximum number of simultaneous trips across all times. Then, we scale down the mean of trip arrivals for all origin-destination pairs at all times based on the ratio of our chosen fleet size (i.e. 300) to the actual estimated fleet size (i.e. 12.8k). We calibrate the battery consumption b_{uv} for each origin u and destination v using

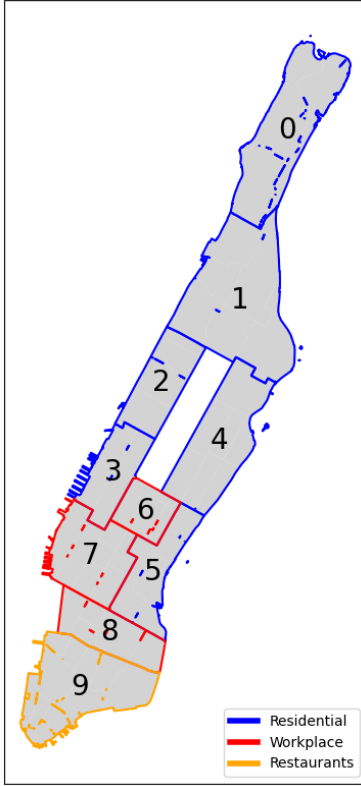


Figure 3: Service Regions in Manhattan.

the Chevrolet Bolt EUV model with battery pack size 65 kW. If fully charged, the range B of the vehicle is 260 miles. For self-driving vehicles, this range is halved because the autonomous driving computation takes around 50% of the battery. We use 75 kW as the outlet rate of DC fast chargers and 15 kW for Level 2 AC (slow) chargers [93, 94].

We adopt the non-linear charging curve for charging (Table 3). Based on the criticality of battery level and the cutoff points of non-linear charging rates, we mark the battery level 0%-10% as “low”, 10%-40% as “medium”, and 40%-100% as “high”. ⁵

We present the details about the neural network architecture and hyper-parameters of Atomic-PPO (see Algorithm 1) in Appendix A. In each experiment, we monitor the training logs of Atomic-PPO and terminate the training when the average reward is no longer improved. In most experiments, Atomic-PPO converges after 10 policy iterations. In policy evaluation, we roll out the Atomic-PPO policy for 10 days per trajectory, collect 10 trajectories, and compute the average daily reward. With 30 CPUs running in parallel, each policy iteration takes 15-20 mins, so the entire training of Atomic-PPO for one problem instance takes 2-3 hours to complete.

We use the power-of- k dispatch policy and the fluid-based policy as our benchmark algorithms. For each trip request, the power-of- k dispatch policy selects the closest k vehicles and assigns the

⁵We remark that due to the decay in charging rate and the large volume of trip demand relative to the fleet size, it is inefficient to fully charge a vehicle.

Parameter	Value
Decision Epoch Length	5 mins
Number of Time Steps Per Day	288
Number of Days Per Episode	8
Fleet Size	300
Battery Pack Size	65 kW
Vehicle Range	130 miles
Initial Vehicle Battery	50% Charged
Charger Outlet Rate	75 kW

Table 2: Simulation environment parameters.

Battery Percentage	0%-10%	10%-40%	40%-60%	60%-80%	80%-90%	90%-95%	95%-100%
Charging Time (s)	47	33	40	60	107	173	533

Table 3: Charging time (seconds) for each percentage of battery increase.

one with the highest battery level to the trip request. If there are no vehicle that can reach the origin of the trip request within L_p units of time, or if none of the k -closest vehicles have enough battery to complete the trip, then the trip request is abandoned. Upon completion of a trip, the vehicle will be routed to the nearest region with chargers. If, at the current decision epoch, the vehicle is not assigned any new trip requests and there is at least one charger unoccupied, then it will be plugged into that charger and charge for one time step. If all chargers are currently occupied or if the vehicle is fully-charged, then the vehicle will idle for one decision epoch. The power-of- k dispatch policy is an intuitive policy and is easy to implement. Under restrictive assumptions where all trip requests and charging facilities are uniformly distributed across the entire service area, [10] proved that the power-of- k dispatch policy achieves the optimal service level measured by the average fraction of trip demand served in the long-run. However, the uniform distribution assumption is not satisfied in our setting. We experiment the power-of- k dispatch policy with $k = 1, \dots, 5$ and we find $k = 2$ to achieve the highest average reward. For the fluid policy, we use the optimal solution of (Fluid-LP) to infer the number of vehicles assigned to each action. Since the LP solution is fractional, we apply randomized rounding to construct a feasible integer policy. Although the fluid-based policy is optimal in the fluid limit, it is suboptimal when the fleet size is finite.

In Section 6.1, we compare the long-run reward achieved by our Atomic-PPO algorithm with the fluid-based reward upper bound \bar{R} and the average reward achieved by the power-of- k dispatch policy and the fluid policy. In Section 6.2, we run our Atomic-PPO algorithm on multiple instances with different number of chargers and different locations of chargers. We draw insight on how the quantity and location of charging facility can impact the reward. For all experiments above, we use DC fast chargers. In Section 6.3, we study how the vehicle range and charging rate affect the

average reward achieved by the algorithm.

6.1 Experiments with Abundant Chargers

For experiments in this section, we assume that there are abundant (300) chargers in each region, so chargers are always available in all regions at all times.

Atomic-PPO achieves high percentage of fluid upper bound and significantly beats benchmark algorithms. Table 4 shows that Atomic-PPO outperforms both the fluid policy and the power-of- k policy by a large margin. After 10 policy iterations, Atomic-PPO achieves an average reward of 91% of the fluid upper bound. In contrast, the power-of- k policy achieves 71%, while the fluid policy performs the worst, reaching only 43% of the fluid upper bound.

Algorithm	Reward/ \bar{R}	Avg. Daily Reward
Atomic-PPO	91%	\$390K
Power of k	71%	\$305K
Fluid policy	43%	\$185K

Table 4: Reward achieved by Atomic-PPO, power-of-k policy and fluid policy.

Atomic-PPO assigns a higher fraction of fleet to trip fulfillment. Figures 4a-4c illustrate the fraction of fleet assigned to each action under Atomic-PPO, power-of- k dispatch, and fluid policies, respectively. The policy trained by the Atomic-PPO algorithm maintains the highest fraction of fleet assigned to trip fulfillment throughout most hours of the day, compared to the other two policies. This indicates that Atomic-PPO fulfills the greatest number of trip requests. Between 9 a.m. and 9 p.m., when the trip arrival rate is relatively high, nearly all vehicles are assigned to serve trip requests under the Atomic-PPO policy. However, a significant fraction of vehicles remain idle throughout the day under both the power-of- k dispatch policy and the fluid policy. The power-of- k policy does not allow for vehicle repositioning. When there is a strong demand imbalance (Figure 2), the power-of- k policy cannot move vehicles from over-supplied regions to pick up trip requests in under-supplied regions. On the other hand, the fluid policy does not adapt to the stochasticity of trip request arrivals, as it is state-independent. When the number of trip arrivals significantly exceeds its Poisson arrival mean, the fluid policy fails to adjust its assignments to accommodate the additional trip requests.

Atomic-PPO fulfills more trips at all times. Figures 5a-5c illustrate the number of fulfilled, queued and abandoned trip requests across all times of a day given the Atomic-PPO policy, the power-of- k dispatch policy, and the fluid policy, respectively. Atomic-PPO consistently fulfills a higher number of trip requests throughout the day compared to both the power-of- k and fluid

policies. While the power-of- k dispatch policy can fulfill nearly all trip requests during the early morning hours (0–6 a.m.) when demand is low, it fulfills significantly fewer requests than Atomic-PPO after 9 a.m. as demand increases. In contrast, the fluid policy fulfills the fewest trip requests at all times of the day, even abandoning some requests during low-demand periods in the early morning.

6.2 Deployment of Charging Facilities

Region	Residential					Workplace			9	Avg. Daily Reward
	0	1	2	3	4	5	6	7		
Unif. 10 chargers	1	1	1	1	1	1	1	1	1	\$250K
Unif. 20 chargers	2	2	2	2	2	2	2	2	2	\$375K
Unif. 30 chargers	3	3	3	3	3	3	3	3	3	\$390K
Unif. 40 chargers	4	4	4	4	4	4	4	4	4	\$390K
Midtown Manhattan.	0	0	0	0	0	0	0	15	0	\$380K
Upper Manhattan	3	3	3	3	3	0	0	0	0	\$225K
Lower Manhattan	0	0	0	0	0	3	3	3	3	\$335K
Abundant Chargers	300	300	300	300	300	300	300	300	300	\$390K
Fluid Upper Bound	300	300	300	300	300	300	300	300	300	\$430K

Table 5: Average daily reward under different charging facility allocations.

We conduct experiments to study how charger deployments affect the average reward. We begin by experimenting with a uniform deployment of chargers across the 10 regions and compute the reward achieved by our Atomic-PPO training algorithm. Starting with 1 charger per region (10 chargers in total), we increase the number of chargers per region by 1 until the average reward matches that achieved by the Atomic-PPO algorithm in the setting with abundant chargers, as shown in Section 6.1. Additionally, we investigate three nonuniform charger deployment settings: (i) allocating 15 chargers in zone 7 of Midtown Manhattan, (ii) allocating 3 chargers in each one of the five zones 0, 1, 2, 3, and 4 of Upper Manhattan, and (iii) allocating 3 chargers in each of the five zones 5, 6, 7, 8, 9 of Lower Manhattan. The average reward achieved by Atomic-PPO under each deployment is summarized in Table 5.

Table 5 demonstrates that achieving the same average reward as the abundant-charger scenario requires 30 chargers when deployed uniformly. With 20 uniformly deployed chargers, the system attains approximately 95% of the reward, whereas performance drops to around 65% with only 10 chargers. In contrast, targeted deployment significantly improves efficiency: allocating 15 chargers uniformly within Lower Manhattan achieves 88% of the reward, while allocating all chargers to Midtown Manhattan yields 98%. As illustrated in Figure 2, Midtown is the most popular destination during morning rush hours and becomes the most frequent origin in the evening. Concentrating

chargers in this region reduces vehicle travel time for recharging, as vehicles can charge in Midtown between the morning and evening peak periods.

6.3 Vehicle Range and Charger Outlet Rates

In Table 6, we compute the average reward achieved by atomic PPO in experiments where all chargers are slow (15 kW) or all vehicles have doubled the range.

Fast chargers can effectively increase the reward, while doubling the vehicle range cannot. Table 6 shows that replacing fast chargers with slow chargers results in a 14% reduction in average daily reward, whereas doubling the vehicle range has minimal impact. This difference arises from the opportunity cost incurred during charging, as vehicles cannot serve trip requests while recharging. Fast chargers reduce this cost by minimizing charging time, enabling quicker return to service. In contrast, increasing vehicle range does not shorten the time required to replenish the same amount of energy and therefore does not reduce the opportunity cost. Furthermore, range has limited influence in the Manhattan region, where most trips have relatively short distances.

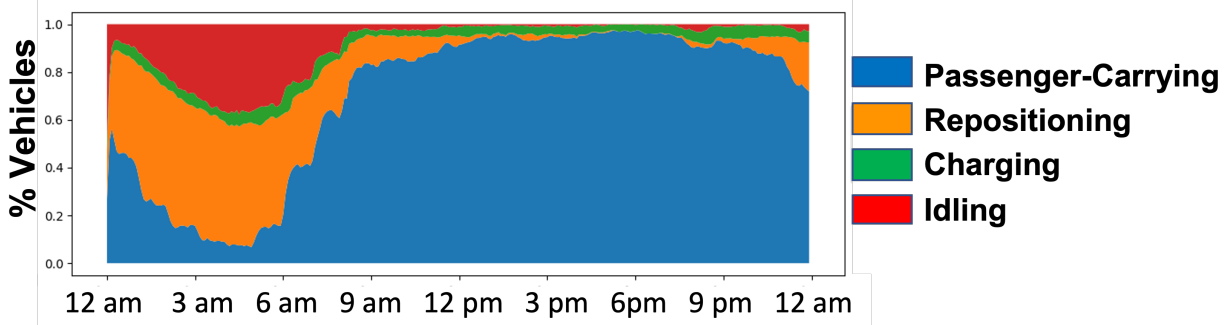
Regime	Charger Power Rates	Vehicle Range	Avg. Daily Reward
Benchmark	75 kW	130 miles	\$390K
Slow Chargers	15 kW	130 miles	\$335K
Double Range	75 kW	260 miles	\$390K

Table 6: Impact of charging rate and vehicle range on average reward.

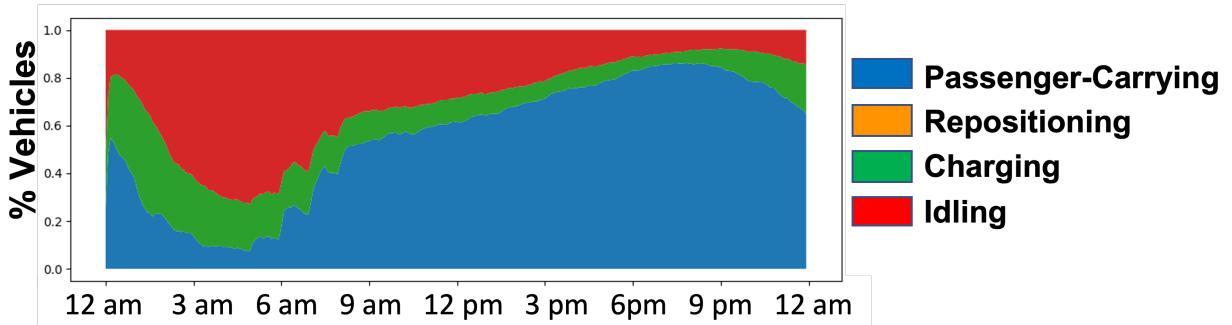
7 Concluding Remarks

In this article, we propose a scalable deep reinforcement learning algorithm – Atomic-PPO – to optimize the long-run average reward of a robo-taxi system. Atomic-PPO integrates an atomic action decomposition into Proximal Policy Optimization (PPO), a state-of-the-art reinforcement learning algorithm. Our atomic action decomposition reduces the action space from exponential in fleet size to constant, which significantly lowers the complexity of policy training. In parallel, our state reduction substantially decreases the input dimension to the neural network and leads to improvements in both runtime and memory. We evaluate our approach through extensive numerical experiments using the NYC for-hire vehicle dataset. Atomic-PPO consistently outperforms benchmark policies in reward maximization. Furthermore, we investigate the impact of charger allocation, vehicle range, and charger rates on the achieved average reward. Our results show that allocating chargers based on ridership patterns yields better outcomes than uniform placement across regions. We also find that investing in fast chargers is critical for performance, whereas extending vehicle range is

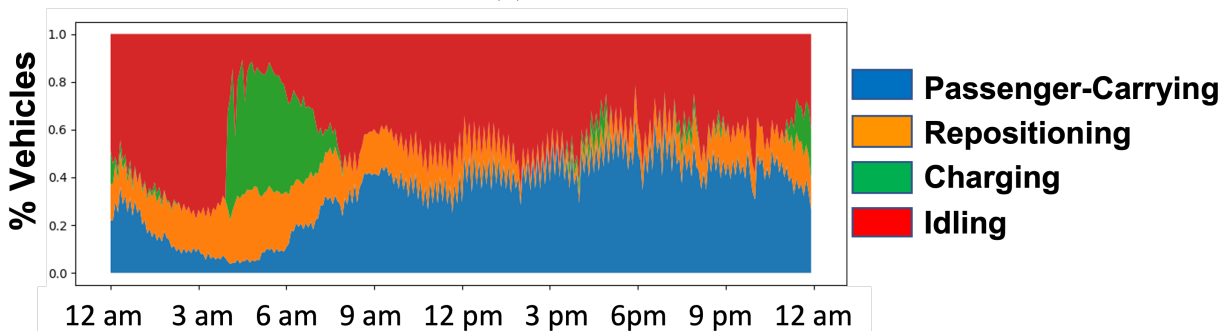
comparatively less important. For future research, we aim to extend Atomic-PPO to broader vehicle routing applications, including delivery and logistics systems.



(a) Atomic-PPO



(b) Power-of-k policy



(c) Fluid Policy

Figure 4: Fleet status of Atomic-PPO, power-of-k dispatch policy, and fluid policy.

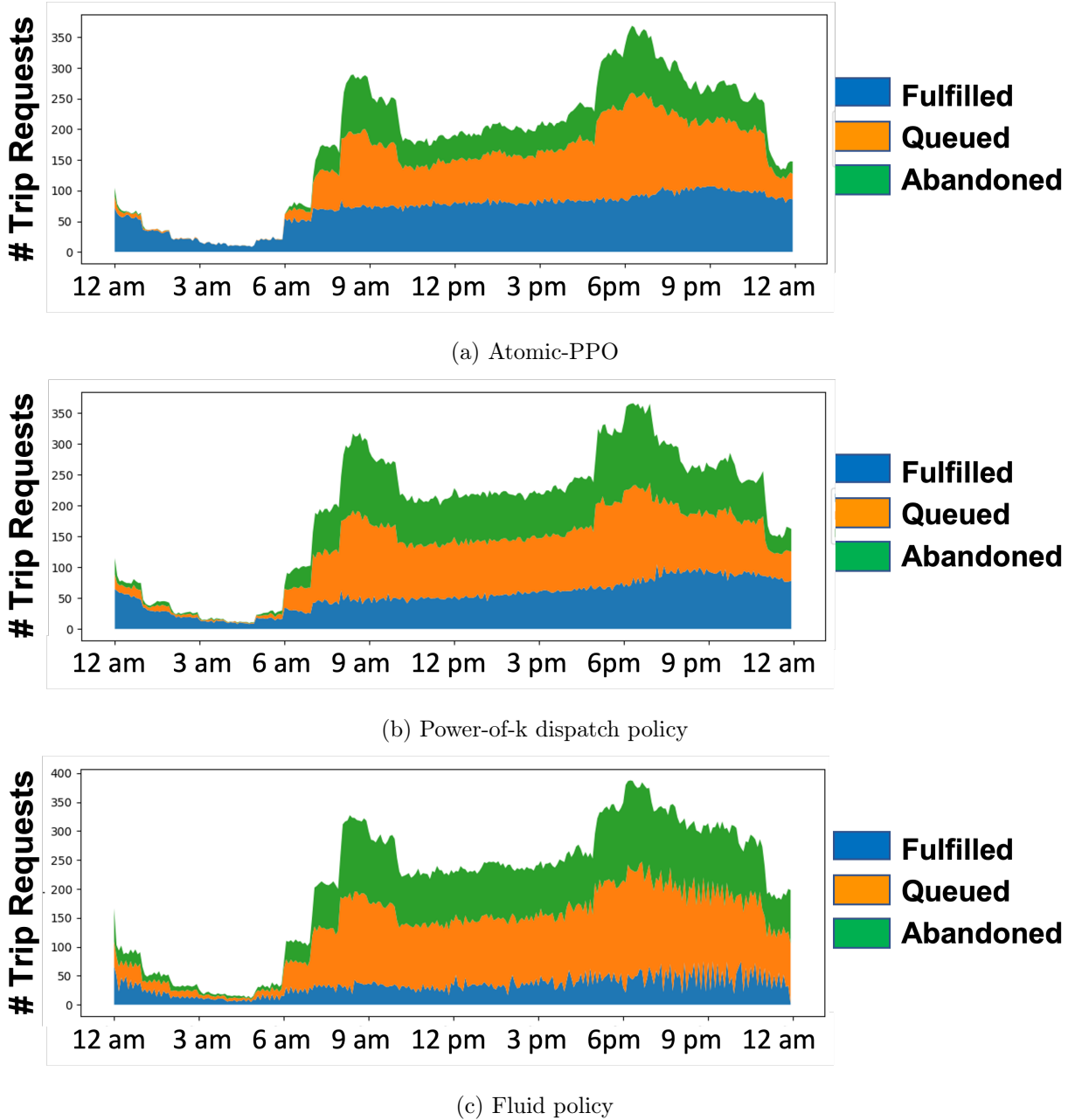


Figure 5: Trip fulfillment under Atomic-PPO policy, power-of-k dispatch policy, and fluid policy.

A Neural Network Parameters

We use deep neural networks to approximate the policy function and the value function. Both policy and value networks consist of a list of 3-layer shallow feed-forward networks, with each shallow network corresponding to a specific time of day. The activation functions of the 3-layer shallow networks for the policy network are tanh, tanh, and tanh. The activation functions of the shallow networks for the value network are tanh, relu, and tanh.

We set the clip parameters with an exponential decay rate. Specifically, let ϵ be the initial clip parameter, and γ be the decay factor. In policy iteration m , the clip parameter is $\max\{\epsilon \cdot \gamma^m, 0.01\}$. The policy and value networks are trained using the Adam solver. We use mini-batch training: in each update step, we randomly sample a batch of data and update the neural network parameters using the gradient computed from this batch. Table 7 specifies the training hyperparameters for the policy and value networks.

Hyperparameter	Value
Number of trajectories per policy iteration	30
Initial clipping size	0.1
Clipping decay factor	0.97
Learning rate for policy network	5e-4
Batch size for policy network	1024
Number of parameter update steps for policy network	20
Learning rate for value network	3e-4
Batch size for value network	1024
Number of parameter update steps for value network	100

Table 7: Hyperparameters for training Atomic PPO

B Proof of Theorem 1

By Theorem 9.1.8 on page 451 of [91], we know that there exists an optimal policy that is deterministic. Therefore, we only need to show that for any arbitrary deterministic stationary policy π , its long-run average daily reward $R(\pi|s)$ is upper bounded by the fluid-based LP optimal objective value \bar{R} . Denote $(f(s^t), e(s^t), q(s^t), i(s^t), p(s^t))$ as a deterministic flow of vehicles generated by policy π given state s^t at time step t . Since the state space of the MDP is finite, we know that given any initial state $s \in \mathcal{S}$ and any deterministic stationary policy π , the system has a stationary state distribution, denoted as ρ . Here, the dependence of ρ on the policy π and the initial state s is dropped for notation simplicity. By proposition 8.1.1 in page 333 of [91], the long-run average daily

reward defined in (13) can be written as follows:

$$\begin{aligned}
R(\pi|s) = & \mathbb{E}_\rho \left[\sum_{t \in [T]} \sum_{c \in \mathcal{C}} \sum_{(u,v) \in V \times V} \right. \\
& \left(r_{f,uv}^t \sum_{\xi \in [L_c]} f_{c,(u,v,\xi)}(s^t) + r_{e,uv}^t e_{c,v}(s^t) \right) \\
& \left. + \sum_{c \in \mathcal{C}} \sum_{\delta \in \Delta} r_{q,\delta}^t q_{c,\delta}(s^t) \right].
\end{aligned}$$

Given $(f(s^t), e(s^t), q(s^t), i(s^t), p(s^t))$ for each state s^t at each time step $t \in [T]$, we define the fleet dispatch fraction vector $(\bar{f}^t, \bar{e}^t, \bar{q}^t, \bar{p}^t)$ for each $t \in [T]$:

- (i) $\bar{f}_{c,o}^t := \frac{1}{N} \mathbb{E}_\rho[f_{c,o}(s^t)]$, $\forall c \in \mathcal{C}$, $o \in \mathcal{O}$, and $t \in [T]$,
- (ii) $\bar{e}_{c,v}^t := \frac{1}{N} \mathbb{E}_\rho[e_{(u,0,b),v}(s^t)]$, $\forall c := (u, 0, b) \in \mathcal{C}$, $v \in V$, $v \neq u$, and $t \in [T]$,
- (iii) $\bar{e}_{(v,0,b),v}^t := \frac{1}{N} \mathbb{E}_\rho[p_{(v,0,b)}(s^t)]$, $\forall c := (v, 0, b) \in \mathcal{C}$, $v \in V$, and $t \in [T]$,
- (iv) $\bar{q}_{c,\delta}^t := \frac{1}{N} \mathbb{E}_\rho[q_{c,\delta}(s^t)]$, $\forall c \in \mathcal{C}$, $\delta \in \Delta$, and $t \in [T]$,
- (v) $\bar{p}_c^t := \frac{1}{N} \mathbb{E}_\rho[p_c(s^t)]$, $\forall c \in \mathcal{C}$ and $t \in [T]$,

where the expectations are taken over the states s^t . First, given that $(f(s^t), e(s^t), q(s^t), i(s^t), p(s^t))$ is a feasible fleet flow that satisfies all constraints in Sec. 2, we show that $(\bar{f}, \bar{e}, \bar{q}, \bar{p})$ is a feasible solution to the fluid-based LP.

We show that constraint (22) holds. The left-hand side aggregates all vehicles from $t-1$ that transitions to status c , while the right-hand side aggregates vehicles of status c assigned to take all actions at time t . Both sides equal to the fraction of vehicles with status c at time t , and thus (22) holds.

Next, we show that constraint (23) holds. By (10), we obtain that for any $u, v \in V$ and any $t \in [T]$,

$$\begin{aligned}
0 & \stackrel{(a)}{\leq} s_{(u,v,L_c)}^t - \sum_{c \in \mathcal{C}} f_{c,(u,v,L_c)}(s^t) \\
& \stackrel{(b)}{=} s_{(u,v,L_c-1)}^{t-1} - \sum_{c \in \mathcal{C}} \left(f_{c,(u,v,L_c)}(s^t) + f_{c,(u,v,L_c-1)}(s^{t-1}) \right) \\
& = \dots \\
& \stackrel{(c)}{=} s_{(u,v,0)}^{t-L_c} - \sum_{c \in \mathcal{C}} \sum_{\xi \in [L_c]} f_{c,(u,v,L_c-\xi)}(s^{t-\xi}) \\
& \stackrel{(d)}{\leq} X_{uv}^{t-L_c} - \sum_{c \in \mathcal{C}} \sum_{\xi \in [L_c]} f_{c,(u,v,L_c-\xi)}(s^{t-\xi}),
\end{aligned}$$

where (a) is due to constraint (4); (b) and (c) are obtained by (10) under the condition that $1 \leq \xi \leq L_c$; and (d) is because the trip state $s_{(u,v,0)}^{t-L_c}$ is upper bounded by $X_{uv}^{t-L_c}$ as in (10) for $\xi = 0$. Thus, we obtain

$$\begin{aligned} X_{uv}^{t-L_c} &\geq \sum_{c \in \mathcal{C}} \sum_{\xi \in [L_c]} f_{c,(u,v,L_c-\xi)}(s^{t-\xi}) \\ &= \sum_{b \in [B]} \sum_{\eta \in [L_p]} \sum_{\xi \in [L_c]} f_{(u,\eta,b),(u,v,L_c-\xi)}(s^{t-\xi}). \end{aligned}$$

We shift t to be $t + L_c$, then the above inequality can be re-written as follows:

$$\begin{aligned} &\frac{1}{N} X_{uv}^t \\ &\geq \frac{1}{N} \sum_{b \in [B]} \sum_{\eta \in [L_p]} \sum_{\xi \in [L_c]} f_{(u,\eta,b),(u,v,L_c-\xi)}(s^{t+L_c-\xi}) \\ &= \frac{1}{N} \sum_{b \in [B]} \sum_{\eta \in [L_p]} \sum_{\xi \in [L_c]} f_{(u,\eta,b),(u,v,\xi)}(s^{t+\xi}), \end{aligned}$$

where the second equation is due to swapping $L_c - \xi$ as ξ . Taking expectation on both sides, we obtain

$$\begin{aligned} \frac{1}{N} \lambda_{uv}^t &= \mathbb{E}_\rho \left[\frac{1}{N} X_{uv}^t(s^t) \right] \\ &\geq \frac{1}{N} \mathbb{E}_\rho \left[\sum_{b \in [B]} \sum_{\eta \in [L_p]} \sum_{\xi \in [L_c]} f_{(u,\eta,b),(u,v,\xi)}(s^{t+\xi}) \right] \\ &= \sum_{b \in [B]} \sum_{\eta \in [L_p]} \sum_{\xi \in [L_c]} \mathbb{E}_\rho \left[\frac{1}{N} f_{(u,\eta,b),(u,v,\xi)}(s^{t+\xi}) \right] \\ &= \sum_{c=(u,\eta,b) \in \mathcal{C}} \sum_{o=(u,v,\xi) \in \mathcal{O}} \bar{f}_{c,o}^{t+\xi}. \end{aligned}$$

The constraint (24) holds because:

$$\begin{aligned} &\sum_{j \in [J]} \sum_{c=(v,0,b) \in \mathcal{C}} \bar{q}_{c,\delta}^{t-j} \\ &= \frac{1}{N} \mathbb{E}_\rho \left[\sum_{j \in [J]} \sum_{c=(v,0,b) \in \mathcal{C}} q_{c,\delta}(s^{t-j}) \right] \\ &\stackrel{(a)}{=} \frac{1}{N} \sum_{j=0}^{J-1} s_{(u,\delta,J-1)}^{t-j} \\ &\stackrel{(b)}{=} \frac{1}{N} s_{(u,\delta,1)}^{t-1} + \frac{1}{N} \sum_{j=1}^{J-1} s_{(u,\delta,j)}^t \\ &\stackrel{(c)}{\leq} \frac{1}{N} s_{(u,\delta,0)}^t + \frac{1}{N} \sum_{j=1}^{J-1} s_{(u,\delta,j)}^t \\ &\stackrel{(d)}{=} \frac{1}{N} n_v^\delta, \end{aligned}$$

where (a) is obtained by the case of $j = J - 1$ in (11); (b) is obtained by the case of $0 < j < J - 1$ in (11); (c) is obtained by the case of $j = 0$ in (11) and the constraint in (7); and (d) is obtained by (2).

Constraints (25) and (26) can be obtained by the constraints (3) and (5) in Sec. 2. Constraint (27) holds due to (1). Finally, constraint (28) holds because the number of fleet assigned to each action must be non-negative. Hence, we obtain that $(\bar{f}(s^t), \bar{e}(s^t), \bar{q}(s^t), \bar{p}(s^t))_{s^t \in S, t \in [T]}$ is a feasible solution of the fluid-based LP (Fluid-LP).

Therefore, we have

$$\begin{aligned}
R(\pi|s) &= \mathbb{E}_\rho \left[\sum_{t \in [T]} \sum_{c \in \mathcal{C}} \sum_{(u,v) \in V \times V} \right. \\
&\quad \left(r_{f,uv}^t \sum_{\xi \in [L_c]} f_{c,(u,v,\xi)}(s^t) + r_{e,uv}^t e_{c,v}(s^t) \right) \\
&\quad + \sum_{c \in \mathcal{C}} \sum_{\delta \in \Delta} r_{q,\delta}^t q_{c,\delta}(s^t) \Big] \\
&\stackrel{(a)}{=} \sum_{t \in [T]} \sum_{c \in \mathcal{C}} \sum_{(u,v) \in V \times V} \\
&\quad \left(r_{f,uv}^t \sum_{\xi \in [L_c]} \mathbb{E}_\rho [f_{c,(u,v,\xi)}(s^t)] \right. \\
&\quad + r_{e,uv}^t \mathbb{E}_\rho [e_{c,v}(s^t)] \\
&\quad + \sum_{c \in \mathcal{C}} \sum_{\delta \in \Delta} r_{q,\delta}^t \mathbb{E}_\rho [q_{c,\delta}(s^t)] \Big] \\
&\stackrel{(b)}{=} N \cdot \left[\sum_{t \in [T]} \sum_{c \in \mathcal{C}} \sum_{(u,v) \in V \times V} \right. \\
&\quad \left(r_{f,uv}^t \sum_{\xi \in [L_c]} \bar{f}_{c,(u,v,\xi)}^t + r_{e,uv}^t \bar{e}_{c,v}^t \right) \\
&\quad + \sum_{c \in \mathcal{C}} \sum_{\delta \in \Delta} r_{q,\delta}^t \bar{q}_{c,\delta}^t \Big] \\
&\stackrel{(c)}{\leq} \bar{R},
\end{aligned}$$

where (a) is obtained by the linearity of expectation, (b) is by plugging in (i)-(v) above, (c) is because $(\bar{f}, \bar{e}, \bar{\mu}, \bar{q}, \bar{p})$ is a feasible solution to the fluid-based LP. As a result, the associated reward function value is upper bounded by the optimal value \bar{R} . \square

C Reduction of Fluid Based Linear Program

In this section, we reformulate (Fluid-LP) to obtain a linear program with fewer decision variables and constraints. This reformulation is achieved based on the fact that only vehicles with task remaining time $\eta \leq L_p$ can be assigned with new tasks, and therefore we only need to keep track of the statuses of vehicles with task remaining time $\eta \leq L_p$ in the optimization formulation. We define the variables of the simplified fluid-based optimization problem as follows:

- *Fraction of fleet for trip fulfilling* $\bar{f}^\dagger := \left(\bar{f}_{uv,b,\eta}^{\dagger t} \right)_{u,v \in V, t \in [T], b \in [B], \eta \in [L_p]}$, where $\bar{f}_{uv,b,\eta}^{\dagger t}$ is the fraction of vehicles with battery level b at time t that pick up trip requests from u to v with remaining waiting time η . We remark two differences between \bar{f}^\dagger and \bar{f} in the original formulation: (i) \bar{f}^\dagger only keeps track of vehicles with task remaining time $\eta \leq L_p$, whereas \bar{f} keeps track of all trip-fulfilling vehicles; (ii) \bar{f}^\dagger aggregates \bar{f} across all trip active times ξ , i.e., $\bar{f}_{uv,b,\eta}^{\dagger t} = \sum_{\xi \in [L_c]} \bar{f}_{(u,\eta,b),(u,v,\xi)}^t$.
- *Fraction of fleet fulfilling trip requests with a certain status* $\bar{\mu}^\dagger := \left(\bar{\mu}_{uv,\eta,\xi}^{\dagger t} \right)_{u,v \in V, \eta \in [L_p], \xi \in [L_c], t \in [T]}$, where $\bar{\mu}_{uv,\eta,\xi}^{\dagger t}$ is fraction of vehicles assigned at time t to a trip with o-d pair uv that has been waiting for assignment for ξ steps and will be picked up after η time steps. We note that $\bar{\mu}^\dagger$ differs from \bar{f}^\dagger in that $\bar{\mu}^\dagger$ aggregates the trip-fulfilling vehicles across battery level b , while \bar{f}^\dagger aggregates them across trip active time ξ . In particular, $\bar{\mu}_{uv,\eta,\xi}^t = \sum_{b \in [B]} \bar{f}_{(u,\eta,b),(u,v,\xi)}^t$.
- *Fraction of repositioning fleet* $\bar{e}^\dagger := \left(\bar{e}_{uv,b}^{\dagger t} \right)_{u,v \in V, t \in [T], b \in [B]}$, where $\bar{e}_{uv,b}^{\dagger t}$ is the fraction of vehicles with battery level b at time t repositioning from u to v . Here, the variable $\bar{e}_{uv,b}^{\dagger t}$ is equivalent to the decision variable $\bar{e}_{(u,0,b),v}^t$ in the original formulation.
- *Fraction of charging fleet* $\bar{q}^\dagger := \left(\bar{q}_{v,\delta,b}^{\dagger t} \right)_{v \in V, \delta \in \Delta, t \in [T], b \in [B]}$, where $\bar{q}_{v,\delta,b}^{\dagger t}$ denotes the fraction of vehicles with battery level b charging at region v with rate δ at time t . Here, the variable $\bar{q}_{v,\delta,b}^{\dagger t}$ is equivalent to the decision variable $\bar{q}_{(v,0,b),\delta}^t$ in the original formulation.
- *Fraction of fleet for passing action* $\bar{p}^\dagger := \left(\bar{p}_{v,b,\eta}^{\dagger t} \right)_{v \in V, b \in [B], \eta \in [L_p], t \in [T]}$, where $\bar{p}_{v,b,\eta}^{\dagger t}$ is the fraction of fleet η time steps away from destination v with battery b that takes the passing action at time t . Here, the variable $\bar{p}_{v,b,\eta}^{\dagger t}$ is equivalent to the decision variable $\bar{p}_{(v,\eta,b)}^t$ in the original formulation. Again, we note that \bar{p}^\dagger only keeps track of the vehicles statuses with task remaining time $\eta \leq L_p$, while \bar{p} in the original formulation keeps track of all vehicle statuses.

The simplified fluid-based linear program is given as follows:

$$\max_{\bar{f}^\dagger, \bar{e}^\dagger, \bar{q}^\dagger, \bar{\mu}^\dagger, \bar{p}^\dagger} N \sum_{t \in [T]} \left\{ \sum_{u \in V} \sum_{v \in V} [r_f^t]_{uv}$$

$$\begin{aligned}
& \left(\sum_{\xi \in [L_c]} \sum_{\eta \in [L_p]} \bar{\mu}_{uv,\eta,\xi}^{\dagger t} \right) + r_{e,uv}^t \sum_{b \in [B]} \bar{e}_{uv,b}^{\dagger t} \\
& + \sum_{\delta \in \Delta} r_{q,\delta}^t \sum_{v \in V} \sum_{b \in [B]} \bar{q}_{v,\delta,b}^{\dagger t} \Big\}, \\
\text{s.t. } & \left[\sum_{v \in V} \left(\sum_{\eta' \in [L_p]} \bar{f}_{vu,b+b_{vu},\eta'}^{\dagger \phi_{vu}(t,\eta')} \right. \right. \\
& + \bar{e}_{vu,b+b_{vu}}^{\dagger \phi_{vu}(t,0)} \mathbf{1}\{v \neq u\} \Big) \mathbf{1}\{b + b_{vu} \leq B\} \\
& + \sum_{\delta \in \Delta} \bar{q}_{u,\delta,b-\delta J}^{\dagger(t+\eta-J)} \mathbf{1}\{b \geq \delta J\} \\
& + \sum_{\delta \in \Delta} \sum_{b' > B-\delta J} \bar{q}_{u,\delta,b'}^{\dagger(t+\eta-J)} \mathbf{1}\{b = B\} \Big] \mathbf{1}\{\eta = L_p\} \\
& + \bar{e}_{uu,b}^{\dagger(t-1)} \mathbf{1}\{\eta = 0\} + \bar{p}_{u,b,\eta+1}^{\dagger(t-1)} \mathbf{1}\{\eta < L_p\} \\
& = \sum_{v \in V} \left(\bar{f}_{uv,b,\eta}^{\dagger t} + \bar{e}_{uv,b}^{\dagger t} \right) + \sum_{\delta \in \Delta} \bar{q}_{u,\delta,b}^{\dagger t} + \bar{p}_{u,b,\eta}^{\dagger t} \mathbf{1}\{\eta > 0\}, \\
& \forall u \in V, \eta \in [L_p], t \in [T], b \in [B], \tag{29a}
\end{aligned}$$

$$\sum_{b \in [B]} \bar{f}_{uv,b,\eta}^{\dagger t} = \sum_{\xi \in [L_c]} \bar{\mu}_{uv,\eta,\xi}^{\dagger t}, \tag{29b}$$

$$\forall u, v \in V, \eta \in [L_p], t \in [T], \tag{29b}$$

$$\sum_{\xi \in [L_c]} \sum_{\eta \in [L_p]} \bar{\mu}_{uv,\eta,\xi}^{\dagger(t+\xi)} \leq \frac{1}{N} \lambda_{uv}^t, \quad \forall u, v \in V, t \in [T], \tag{29c}$$

$$\sum_{j \in [J]} \sum_{b \in [B]} \bar{q}_{v,\delta,b}^{\dagger(t-j)} \leq \frac{1}{N} n_v^\delta, \quad \forall \delta \in \Delta, v \in V, t \in [T], \tag{29d}$$

$$\bar{f}_{uv,b,\eta}^{\dagger t} \mathbf{1}\{b < b_{uv}\} = 0, \tag{29e}$$

$$\forall b \in [B], u, v \in V, t \in [T], \eta \in [L_p], \tag{29e}$$

$$\bar{e}_{uv,b}^{\dagger t} \mathbf{1}\{b < b_{uv}\} = 0, \tag{29f}$$

$$\forall b \in [B], u, v \in V, t \in [T], \tag{29f}$$

$$\begin{aligned}
& \sum_{b \in [B]} \left[\sum_{u,v \in V} \left(\sum_{\eta' \in [L_p]} \sum_{t' \in \psi_{uv}(t,\eta')} \bar{f}_{uv,b,\eta'}^{\dagger t'} + \right. \right. \\
& \left. \left. \sum_{t' \in \psi_{uv}(t,0)} \bar{e}_{uv,b}^{\dagger t'} \right) \right. \\
& + \sum_{v \in V} \sum_{\delta \in \Delta} \sum_{t'=t-J+L_p}^t \bar{q}_{v,\delta,b}^{\dagger t'} + \sum_{v \in V} \sum_{\eta \in [L_p]} \bar{p}_{v,b,\eta}^{\dagger t} \Big] = 1, \\
& \forall t \in [T], \tag{29g}
\end{aligned}$$

$$\bar{f}^\dagger, \bar{e}^\dagger, \bar{q}^\dagger, \bar{\mu}^\dagger, \bar{p}^\dagger \geq 0, \tag{29h}$$

where $\phi_{uv}(t, \eta')$ is defined as the time at which the vehicle assigned to a trip from region u to region

v will be L_p time steps away from v at time t :

$$\begin{aligned} \phi_{uv}(t, \eta') + \eta' + \tau_{uv}^{\phi_{uv}(t, \eta') + \eta'} - L_p &= t, \\ \forall u, v \in V, \forall \eta' \in [L_p], \forall t \in [T], \end{aligned} \quad (30)$$

and $\psi_{uv}(t, \eta')$ is defined as the set of times at which the vehicle assigned to a trip from u to v will be *at least* L_p time steps away from v at time t :

$$\begin{aligned} \psi_{uv}(t, \eta') &= \{t' \in [T] | t' \leq t, \\ t' + \eta' + \tau_{uv}^{t' + \eta'} - L_p &\geq t\}. \end{aligned} \quad (31)$$

The objective function represents the daily average reward achieved by the vehicle flow. We argue that this objective function is equivalent to the objective function of the original formulation. For each pair of origin u and destination v at time t , the term $\sum_{\xi \in [L_c]} \sum_{\eta \in [L_p]} \bar{\mu}_{uv, \eta, \xi}^{\dagger t}$ aggregates all vehicles that are assigned to fulfill trip requests from u to v at time t , which is equivalent to the term $\sum_{c \in \mathcal{C}} \sum_{\xi \in [L_c]} \bar{f}_{c, (u, v, \xi)}^t$ in the objective function of the original formulation. The term $\sum_{b \in [B]} \bar{e}_{uv, b}^{\dagger t}$ aggregates all vehicles assigned to reposition from u to v at time t , which is equivalent to the term $\sum_{c \in \mathcal{C}} \bar{e}_{c, v}^t$ in the objective function of the original formulation. Finally, the term $\sum_{b \in [B]} \bar{q}_{v, \delta, b}^{\dagger t}$ aggregates all vehicles assigned to charge at region v with rate δ at time t , which is equivalent to the term $\sum_{c \in \mathcal{C}} \bar{q}_{c, \delta}^t$ in the objective function of the original formulation.

Constraint (29a) ensures the flow conservation for each vehicle status (u, η, b) with $\eta \leq L_p$ at any time t of day. We remark that the constraint (22) in the original formulation also includes the flow conservation for vehicles statuses with $\eta > L_p$. We can reduce these constraints because passing is the only feasible actions for these vehicles. The left-hand side of the equation represents the vehicles being assigned at previous times that reach the status (u, η, b) at time t , which is equivalent to the left-hand side of (22) in the original formulation and can be obtained by the vehicle state transition equation (9). In particular, the left-hand side includes the following terms: (i) the term $\bar{f}_{vu, b+b_{vu}, \eta}^{\dagger \phi_{vu}(t, \eta')}$ represents that vehicles of status $(v, b + b_{vu}, \eta')$ at time $\phi_{vu}(t, \eta')$ become vehicles of status (u, b, η) after being assigned to pick up trip orders from v to u ; (ii) the term $\bar{e}_{vu, b+b_{vu}}^{\dagger \phi_{vu}(t, 0)}$ represents that vehicles of status $(v, b + b_{vu}, 0)$ at time $\phi_{vu}(t, 0)$ become vehicles of status (u, b, η) after being assigned to reposition from v to u if $v \neq u$. On the other hand, when $\eta = 0$, the term $\bar{e}_{uu, b}^{\dagger(t-1)} \mathbf{1}\{\eta = 0\}$ represents that vehicles of status $(u, 0, b)$ at time $t - 1$ remain the same status at time t after being assigned to idle; (iii) the term $\bar{q}_{u, \delta, b-\delta J}^{\dagger(t+\eta-J)}$ represents that vehicles of status $(v, b - b_{vu}, 0)$ at time $t + \eta - J$ become vehicles of status (u, b, η) after being assigned to charge in region u at rate δ . Moreover, the term $\sum_{b' > B - \delta J} \bar{q}_{u, \delta, b'}^{\dagger(t+\eta-J)}$ represents that if $b = B$, all vehicles of status $(u, b', 0)$ with battery levels $b' > B - \delta J$ will charge to full and become vehicles of status (u, B, η) after being assigned to charge in region u at rate δ ; (iv) the term $\bar{p}_{u, b, \eta+1}^{\dagger(t-1)}$ represents that vehicles of status $(v, b, \eta + 1)$ assigned a passing action at time $t - 1$ become vehicles of status (v, b, η) at time t . The right hand side of (29a) represents the outgoing vehicle flows for each vehicle status, which can be obtained by (8) and is equivalent to the right-hand side of (22).

Constraint (29b) represents the equivalence of two aggregations of trip-fulfilling vehicle flows, which is reflected by the definition of \bar{f}^\dagger and $\bar{\mu}^\dagger$ at the beginning of this section. Constraint (29c) ensures that the fulfillment of trip orders does not exceed their arrivals, which is equivalent to the constraint (23) in the original formulation. Constraints (29e) and (29f) ensure that vehicles will not travel to some regions if their battery levels are below the battery cost required to complete the trip, which are equivalent to the constraints (25) and (26) in the original formulation.

Constraint (29g) ensures that the total fraction of vehicles should add up to 1 at all times and is equivalent to the constraint (27) in the original formulation. At each time, a vehicle can either be dispatched to pick up trip requests, reposition, charge, pass, continue with ongoing trips, or continue being charged. $\psi_{uv}(t, \eta')$ represents the time steps at which vehicles η' away from u and assigned to pick up trip requests from u to v will still be more than L_p time steps away from reaching v at time t . In other words, these vehicles are not feasible for non-passing actions at time t . In particular, the constraint (29g) includes the following terms: (i) the term $\sum_{\eta' \in [L_p]} \sum_{t' \in \psi_{uv}(t, \eta')} \bar{f}_{uv, b, \eta'}^{\dagger t'}$ represents all vehicles assigned to pickup trip requests from u to v that are still more than L_p time steps away from reaching v at time t ; (ii) the term $\sum_{t' \in \psi_{uv}(t, 0)} \bar{e}_{uv, b}^{\dagger t'}$ represents all vehicles assigned to reposition from u to v that are still more than L_p time steps away from reaching v at time t ; (iii) the term $\sum_{t'=t-J+L_p}^t \bar{q}_{v, \delta, b}^{\dagger t'}$ represents all vehicles assigned to charge in region v with rate δ that are still more than L_p time steps away from completing their charging periods; (iv) the term $\sum_{v \in V} \sum_{\eta \in [L_p]} \bar{p}_{v, b, \eta}^{\dagger t}$ represents all vehicles assigned to pass at time t .

The constraint (29h) requires that all decision variables should be non-negative, which is equivalent to the constraint (28) in the original formulation.

References

- [1] Martine Paris. How robotaxis are trying to win passengers' trust. <https://www.bbc.com/future/article/20241115-how-robotaxis-are-trying-to-win-passengers-trust>, 2024.
- [2] John Schulman, Filip Wolski, Prafulla Dhariwal, Alec Radford, and Oleg Klimov. Proximal policy optimization algorithms. *arXiv preprint arXiv:1707.06347*, 2017.
- [3] Oriol Vinyals, Igor Babuschkin, Wojciech M Czarnecki, Michaël Mathieu, Andrew Dudzik, Junyoung Chung, David H Choi, Richard Powell, Timo Ewalds, Petko Georgiev, et al. Grandmaster level in starcraft ii using multi-agent reinforcement learning. *nature*, 575(7782):350–354, 2019.
- [4] Christopher Berner, Greg Brockman, Brooke Chan, Vicki Cheung, Przemysław Dębiak, Christy Dennison, David Farhi, Quirin Fischer, Shariq Hashme, Chris Hesse, et al. Dota 2 with large scale deep reinforcement learning. *arXiv preprint arXiv:1912.06680*, 2019.
- [5] Gregor Simm, Robert Pinsler, and José Miguel Hernández-Lobato. Reinforcement learning for molecular design guided by quantum mechanics. In *International Conference on Machine Learning*, pages 8959–8969. PMLR, 2020.
- [6] Barret Zoph, Vijay Vasudevan, Jonathon Shlens, and Quoc V Le. Learning transferable architectures for scalable image recognition. In *Proceedings of the IEEE conference on computer vision and pattern recognition*, pages 8697–8710, 2018.
- [7] Ilge Akkaya, Marcin Andrychowicz, Maciek Chociej, Mateusz Litwin, Bob McGrew, Arthur Petron, Alex Paino, Matthias Plappert, Glenn Powell, Raphael Ribas, et al. Solving rubik's cube with a robot hand. *arXiv preprint arXiv:1910.07113*, 2019.
- [8] NYC-TLC. New york city taxi and limousine commission. <https://www.nyc.gov/site/tlc/about/tlc-trip-record-data.page>, 2023. Accessed: 2023-06-04.
- [9] Bigad Shaban. Waymo waitlist over in san francisco; all can hail driverless cars. <https://www.nbcbayarea.com/news/local/san-francisco/waymo-waitlist-over-sf/3574655/>, 2024.
- [10] Sushil Mahavir Varma, Francisco Castro, and Siva Theja Maguluri. Electric vehicle fleet and charging infrastructure planning. *arXiv preprint arXiv:2306.10178*, 2023.
- [11] Nikita Dmitrievna Vvedenskaya, Roland L'vovich Dobrushin, and Fridrikh Izrailevich Karpelevich. Queueing system with selection of the shortest of two queues: An asymptotic approach. *Problemy Peredachi Informatsii*, 32(1):20–34, 1996.

[12] Michael Mitzenmacher. Load balancing and density dependent jump markov processes. In *Proceedings of 37th Conference on Foundations of Computer Science*, pages 213–222. IEEE, 1996.

[13] Roberto Roberti and Min Wen. The electric traveling salesman problem with time windows. *Transportation Research Part E: Logistics and Transportation Review*, 89:32–52, 2016.

[14] Justin Luke, Mauro Salazar, Ram Rajagopal, and Marco Pavone. Joint optimization of autonomous electric vehicle fleet operations and charging station siting. In *2021 IEEE International Intelligent Transportation Systems Conference (ITSC)*, pages 3340–3347. IEEE, 2021.

[15] Felix Boewing, Maximilian Schiffer, Mauro Salazar, and Marco Pavone. A vehicle coordination and charge scheduling algorithm for electric autonomous mobility-on-demand systems. In *2020 American Control Conference (ACC)*, pages 248–255. IEEE, 2020.

[16] Matthew Zalesak and Samitha Samaranayake. Real time operation of high-capacity electric vehicle ridesharing fleets. *Transportation Research Part C: Emerging Technologies*, 133:103413, 2021.

[17] Jie Shi, Yuanqi Gao, Wei Wang, Nanpeng Yu, and Petros A Ioannou. Operating electric vehicle fleet for ride-hailing services with reinforcement learning. *IEEE Transactions on Intelligent Transportation Systems*, 21(11):4822–4834, 2019.

[18] Nicholas D. Kullman, Martin Cousineau, Justin C. Goodson, and Jorge E. Mendoza. Dynamic ride-hailing with electric vehicles. *Transportation Science*, 56(3):775–794, may 2022. ISSN 1526-5447. doi: 10.1287/trsc.2021.1042. URL <https://doi.org/10.1287/trsc.2021.1042>.

[19] Matthew D Dean, Krishna Murthy Gurumurthy, Felipe de Souza, Joshua Auld, and Kara M Kockelman. Synergies between repositioning and charging strategies for shared autonomous electric vehicle fleets. *Transportation Research Part D: Transport and Environment*, 108:103314, 2022.

[20] Xinlian Yu, Zihao Zhu, Haijun Mao, Mingzhuang Hua, Dawei Li, Jingxu Chen, and Hongli Xu. Coordinating matching, rebalancing and charging of electric ride-hailing fleet under hybrid requests. *Transportation Research Part D: Transport and Environment*, 123:103903, 2023.

[21] Nitish Singh, Alp Akcay, Quang-Vinh Dang, Tugce Martagan, and Ivo Adan. Dispatching agvs with battery constraints using deep reinforcement learning. *Computers & Industrial Engineering*, 187:109678, 2024.

[22] Yuxuan Dong, René De Koster, Debjit Roy, and Yugang Yu. Dynamic vehicle allocation policies for shared autonomous electric fleets. *Transportation Science*, 56(5):1238–1258, 2022.

[23] Yue Su, Nicolas Dupin, Sophie N Parragh, and Jakob Puchinger. A branch-and-price algorithm for the electric autonomous dial-a-ride problem. *Transportation Research Part B: Methodological*, 186:103011, 2024.

[24] Ramin Ahadi, Wolfgang Ketter, John Collins, and Nicolò Daina. Cooperative learning for smart charging of shared autonomous vehicle fleets. *Transportation Science*, 57(3):613–630, 2023.

[25] Shuo Liu, Yunhao Wang, Xu Chen, Yongjie Fu, and Xuan Di. Smart-eflo: An integrated sumo-gym framework for multi-agent reinforcement learning in electric fleet management problem. In *2022 IEEE 25th International Conference on Intelligent Transportation Systems (ITSC)*, pages 3026–3031. IEEE, 2022.

[26] Linji Chen, Homayoun Hamedmoghadam, Mahdi Jalili, and Mohsen Ramezani. Electric vehicle e-hailing fleet dispatching and charge scheduling. *arXiv preprint arXiv:2302.12650*, 2023.

[27] Yutong Gao, Shu Zhang, Zhiwei Zhang, and Quanwu Zhao. The stochastic share-a-ride problem with electric vehicles and customer priorities. *Computers & Operations Research*, 164:106550, 2024.

[28] Xiaoming Li, Hubert Normandin-Taillon, Chun Wang, and Xiao Huang. Bm-rcwtsg: An integrated matching framework for electric vehicle ride-hailing services under stochastic guidance. *Sustainable Cities and Society*, 108:105485, 2024.

[29] Junchi Ma, Yuan Zhang, Zongtao Duan, and Lei Tang. Prolific: Deep reinforcement learning for efficient ev fleet scheduling and charging. *Sustainability*, 15(18):13553, 2023.

[30] Xiaoming Li, Chun Wang, and Xiao Huang. Coordinating guidance, matching, and charging station selection for electric vehicle ride-hailing services through data-driven stochastic optimization. *arXiv preprint arXiv:2401.03300*, 2024.

[31] Xiaolei Zhu, Xindi Tang, Jiaohong Xie, and Yang Liu. Dynamic balancing-charging management for shared autonomous electric vehicle systems: A two-stage learning-based approach. In *2023 IEEE 26th International Conference on Intelligent Transportation Systems (ITSC)*, pages 3762–3769. IEEE, 2023.

[32] Jesper C Provoost, Andreas Kamaris, Gyözö Gidófalvi, Geert J Heijenk, and Luc JJ Wismans. Improving operational efficiency in ev ridepooling fleets by predictive exploitation of idle times. *arXiv preprint arXiv:2208.14852*, 2022.

[33] Lina Al-Kanj, Juliana Nascimento, and Warren B Powell. Approximate dynamic programming for planning a ride-hailing system using autonomous fleets of electric vehicles. *European Journal of Operational Research*, 284(3):1088–1106, 2020.

[34] Riccardo Iacobucci, Benjamin McLellan, and Tetsuo Tezuka. Optimization of shared autonomous electric vehicles operations with charge scheduling and vehicle-to-grid. *Transportation Research Part C: Emerging Technologies*, 100:34–52, 2019.

[35] Charly Robinson La Rocca and Jean-François Cordeau. Heuristics for electric taxi fleet management at teo taxi. *INFOR: Information Systems and Operational Research*, 57(4):642–666, 2019.

[36] Berkay Turan, Ramtin Pedarsani, and Mahnoosh Alizadeh. Dynamic pricing and fleet management for electric autonomous mobility on demand systems. *Transportation Research Part C: Emerging Technologies*, 121:102829, 2020.

[37] Ning Wang and Jiahui Guo. Multi-task dispatch of shared autonomous electric vehicles for mobility-on-demand services—combination of deep reinforcement learning and combinatorial optimization method. *Heliyon*, 8(11), 2022.

[38] Yaofeng Song, Han Zhao, Ruikang Luo, Liping Huang, Yicheng Zhang, and Rong Su. A sumo framework for deep reinforcement learning experiments solving electric vehicle charging dispatching problem. *arXiv preprint arXiv:2209.02921*, 2022.

[39] Kerem Tuncel, Haris N Koutsopoulos, and Zhenliang Ma. An integrated ride-matching and vehicle-rebalancing model for shared mobility on-demand services. *Computers & Operations Research*, 159:106317, 2023.

[40] Siddhartha Banerjee, Yash Kanoria, and Pengyu Qian. State dependent control of closed queueing networks. *SIGMETRICS Perform. Eval. Rev.*, 46(1):2–4, jun 2018. ISSN 0163-5999. doi: 10.1145/3292040.3219619. URL <https://doi.org/10.1145/3292040.3219619>.

[41] Anton Braverman, Jim G Dai, Xin Liu, and Lei Ying. Empty-car routing in ridesharing systems. *Operations Research*, 67(5):1437–1452, 2019.

[42] Wenbo Zhang, Harsha Honnappa, and Satish V. Ukkusuri. Modeling urban taxi services with e-hailings: A queueing network approach, 2018.

[43] Ariel Waserhole and Vincent Jost. Vehicle sharing system pricing regulation: A fluid approximation. 2012.

[44] Philipp Afèche, Zhe Liu, and Costis Maglaras. Ride-hailing networks with strategic drivers: The impact of platform control capabilities on performance. *Manufacturing & Service Operations Management*, 25(5):1890–1908, sep 2023. ISSN 1526-5498. doi: 10.1287/msom.2023.1221. URL <https://doi.org/10.1287/msom.2023.1221>.

[45] Guangju Wang, Hailun Zhang, and Jiheng Zhang. On-demand ride-matching in a spatial model with abandonment and cancellation. *Operations Research*, 11 2022. doi: 10.1287/opre.2022.2399.

- [46] Erhun Özkan. Joint pricing and matching in ride-sharing systems. *European Journal of Operational Research*, 287(3):1149–1160, 2020.
- [47] Erhun Özkan and Amy R Ward. Dynamic matching for real-time ride sharing. *Stochastic Systems*, 10(1):29–70, 2020.
- [48] Zhengtian Xu, Yafeng Yin, Xiuli Chao, Hongtu Zhu, and Jieping Ye. A generalized fluid model of ride-hailing systems. *Transportation Research Part B: Methodological*, 150:587–605, 2021.
- [49] Zhiwei Tony Qin, Hongtu Zhu, and Jieping Ye. Reinforcement learning for ridesharing: An extended survey. *Transportation Research Part C: Emerging Technologies*, 144:103852, 2022.
- [50] R-Julius O Heitmann, Ninja Soeffker, Marlin W Ulmer, and Dirk C Mattfeld. Combining value function approximation and multiple scenario approach for the effective management of ride-hailing services. *EURO Journal on Transportation and Logistics*, 12:100104, 2023.
- [51] Honghao Wei, Zixian Yang, Xin Liu, Zhiwei Qin, Xiaocheng Tang, and Lei Ying. A reinforcement learning and prediction-based lookahead policy for vehicle repositioning in online ride-hailing systems. *IEEE Transactions on Intelligent Transportation Systems*, 2023.
- [52] Enpeng Yuan, Wenbo Chen, and Pascal Van Hentenryck. Reinforcement learning from optimization proxy for ride-hailing vehicle relocation. *Journal of Artificial Intelligence Research*, 75:985–1002, 2022.
- [53] Guoyang Qin, Qi Luo, Yafeng Yin, Jian Sun, and Jieping Ye. Optimizing matching time intervals for ride-hailing services using reinforcement learning. *Transportation Research Part C: Emerging Technologies*, 129:103239, 2021.
- [54] Yang Liu, Fanyou Wu, Cheng Lyu, Shen Li, Jieping Ye, and Xiaobo Qu. Deep dispatching: A deep reinforcement learning approach for vehicle dispatching on online ride-hailing platform. *Transportation Research Part E: Logistics and Transportation Review*, 161:102694, 2022.
- [55] Chao Mao, Yulin Liu, and Zuo-Jun Max Shen. Dispatch of autonomous vehicles for taxi services: A deep reinforcement learning approach. *Transportation Research Part C: Emerging Technologies*, 115:102626, 2020.
- [56] Xiaoting Zhou, Lubin Wu, Yu Zhang, Zhen-Song Chen, and Shancheng Jiang. A robust deep reinforcement learning approach to driverless taxi dispatching under uncertain demand. *Information Sciences*, 646:119401, 2023.
- [57] Monika Filipovska, Michael Hyland, and Haimanti Bala. Anticipatory fleet repositioning for shared-use autonomous mobility services: An optimization and learning-based approach. *arXiv preprint arXiv:2210.08659*, 2022.

[58] Daniele Gammelli, Kaidi Yang, James Harrison, Filipe Rodrigues, Francisco Pereira, and Marco Pavone. Graph meta-reinforcement learning for transferable autonomous mobility-on-demand. In *Proceedings of the 28th ACM SIGKDD Conference on Knowledge Discovery and Data Mining*, pages 2913–2923, 2022.

[59] Eerotokritos Skordilis, Yi Hou, Charles Tripp, Matthew Moniot, Peter Graf, and David Biagioni. A modular and transferable reinforcement learning framework for the fleet rebalancing problem. *IEEE Transactions on Intelligent Transportation Systems*, 23(8):11903–11916, 2021.

[60] Carolin Schmidt, Daniele Gammelli, Francisco Camara Pereira, and Filipe Rodrigues. Learning to control autonomous fleets from observation via offline reinforcement learning. In *2024 European Control Conference (ECC)*, pages 1399–1406. IEEE, 2024.

[61] Jiaohong Xie, Yang Liu, and Nan Chen. Two-sided deep reinforcement learning for dynamic mobility-on-demand management with mixed autonomy. *Transportation Science*, 57(4):1019–1046, 2023.

[62] Jinhua Si, Fang He, Xi Lin, and Xindi Tang. Vehicle dispatching and routing of on-demand intercity ride-pooling services: A multi-agent hierarchical reinforcement learning approach. *Transportation Research Part E: Logistics and Transportation Review*, 186:103551, 2024.

[63] Zhe Xu, Zhixin Li, Qingwen Guan, Dingshui Zhang, Qiang Li, Junxiao Nan, Chunyang Liu, Wei Bian, and Jieping Ye. Large-scale order dispatch in on-demand ride-hailing platforms: A learning and planning approach. In *Proceedings of the 24th ACM SIGKDD international conference on knowledge discovery & data mining*, pages 905–913, 2018.

[64] Zhaodong Wang, Zhiwei Qin, Xiaocheng Tang, Jieping Ye, and Hongtu Zhu. Deep reinforcement learning with knowledge transfer for online rides order dispatching. In *2018 IEEE International Conference on Data Mining (ICDM)*, pages 617–626. IEEE, 2018.

[65] Xiaocheng Tang, Zhiwei Qin, Fan Zhang, Zhaodong Wang, Zhe Xu, Yintai Ma, Hongtu Zhu, and Jieping Ye. A deep value-network based approach for multi-driver order dispatching. In *Proceedings of the 25th ACM SIGKDD international conference on knowledge discovery & data mining*, pages 1780–1790, 2019.

[66] Zhiwei Qin, Xiaocheng Tang, Yan Jiao, Fan Zhang, Zhe Xu, Hongtu Zhu, and Jieping Ye. Ride-hailing order dispatching at didi via reinforcement learning. *INFORMS Journal on Applied Analytics*, 50(5):272–286, 2020.

[67] Miyoung Han, Pierre Senellart, Stéphane Bressan, and Huayu Wu. Routing an autonomous taxi with reinforcement learning. In *Proceedings of the 25th ACM International Conference on Information and Knowledge Management*, pages 2421–2424, 2016.

[68] Jiarui Jin, Ming Zhou, Weinan Zhang, Minne Li, Zilong Guo, Zhiwei Qin, Yan Jiao, Xiaocheng Tang, Chenxi Wang, Jun Wang, et al. Coride: joint order dispatching and fleet management for multi-scale ride-hailing platforms. In *Proceedings of the 28th ACM international conference on information and knowledge management*, pages 1983–1992, 2019.

[69] Minne Li, Zhiwei Qin, Yan Jiao, Yaodong Yang, Jun Wang, Chenxi Wang, Guobin Wu, and Jieping Ye. Efficient ridesharing order dispatching with mean field multi-agent reinforcement learning. In *The world wide web conference*, pages 983–994, 2019.

[70] Ming Zhou, Jiarui Jin, Weinan Zhang, Zhiwei Qin, Yan Jiao, Chenxi Wang, Guobin Wu, Yong Yu, and Jieping Ye. Multi-agent reinforcement learning for order-dispatching via order-vehicle distribution matching. In *Proceedings of the 28th ACM International Conference on Information and Knowledge Management*, pages 2645–2653, 2019.

[71] Tobias Enders, James Harrison, Marco Pavone, and Maximilian Schiffer. Hybrid multi-agent deep reinforcement learning for autonomous mobility on demand systems. In *Learning for Dynamics and Control Conference*, pages 1284–1296. PMLR, 2023.

[72] Edyvalberty Alenquer Cordeiro and Anselmo Ramalho Pitombeira-Neto. Deep reinforcement learning for the dynamic vehicle dispatching problem: An event-based approach. *arXiv preprint arXiv:2307.07508*, 2023.

[73] Jinhao Xi, Fenghua Zhu, Peijun Ye, Yisheng Lv, Haina Tang, and Fei-Yue Wang. Hmdrl: Hierarchical mixed deep reinforcement learning to balance vehicle supply and demand. *IEEE Transactions On Intelligent Transportation Systems*, 23(11):21861–21872, 2022.

[74] Haoyang Chen, Peiyan Sun, Qiyuan Song, Wanyuan Wang, Weiwei Wu, Wencan Zhang, Guanyu Gao, and Yan Lyu. i-rebalance: Personalized vehicle repositioning for supply demand balance. In *Proceedings of the AAAI Conference on Artificial Intelligence*, volume 38, pages 46–54, 2024.

[75] Jinhao Xi, Fenghua Zhu, Yuanyuan Chen, Yisheng Lv, Chang Tan, and Feiyue Wang. Ddrl: A decentralized deep reinforcement learning method for vehicle repositioning. In *2021 IEEE International Intelligent Transportation Systems Conference (ITSC)*, pages 3984–3989. IEEE, 2021.

[76] Huigui Rong, Xun Zhou, Chang Yang, Zubair Shafiq, and Alex Liu. The rich and the poor: A markov decision process approach to optimizing taxi driver revenue efficiency. In *Proceedings of the 25th ACM international conference on information and knowledge management*, pages 2329–2334, 2016.

[77] Xian Yu and Siqian Shen. An integrated decomposition and approximate dynamic programming approach for on-demand ride pooling. *IEEE Transactions on Intelligent Transportation Systems*, 21(9):3811–3820, 2019.

[78] Zhenyu Shou, Xuan Di, Jieping Ye, Hongtu Zhu, Hua Zhang, and Robert Hampshire. Optimal passenger-seeking policies on e-hailing platforms using markov decision process and imitation learning. *Transportation Research Part C: Emerging Technologies*, 111:91–113, 2020.

[79] Xun Zhou, Huigui Rong, Chang Yang, Qun Zhang, Amin Vahedian Khezerlou, Hui Zheng, Zubair Shafiq, and Alex X Liu. Optimizing taxi driver profit efficiency: A spatial network-based markov decision process approach. *IEEE Transactions on Big Data*, 6(1):145–158, 2018.

[80] Zeno Woywood, Jasper I Wiltfang, Julius Luy, Tobias Enders, and Maximilian Schiffer. Multi-agent soft actor-critic with global loss for autonomous mobility-on-demand fleet control. *arXiv preprint arXiv:2404.06975*, 2024.

[81] Tanvi Verma, Pradeep Varakantham, Sarit Kraus, and Hoong Chuin Lau. Augmenting decisions of taxi drivers through reinforcement learning for improving revenues. In *Proceedings of the International Conference on Automated Planning and Scheduling*, volume 27, pages 409–417, 2017.

[82] Yong Gao, Dan Jiang, and Yan Xu. Optimize taxi driving strategies based on reinforcement learning. *International Journal of Geographical Information Science*, 32(8):1677–1696, 2018.

[83] Jian Wen, Jinhua Zhao, and Patrick Jaillet. Rebalancing shared mobility-on-demand systems: A reinforcement learning approach. In *2017 IEEE 20th international conference on intelligent transportation systems (ITSC)*, pages 220–225. Ieee, 2017.

[84] John Holler, Risto Vuorio, Zhiwei Qin, Xiaocheng Tang, Yan Jiao, Tiancheng Jin, Satinder Singh, Chenxi Wang, and Jieping Ye. Deep reinforcement learning for multi-driver vehicle dispatching and repositioning problem. In *2019 IEEE International Conference on Data Mining (ICDM)*, pages 1090–1095. IEEE, 2019.

[85] Yan Jiao, Xiaocheng Tang, Zhiwei Tony Qin, Shuaiji Li, Fan Zhang, Hongtu Zhu, and Jieping Ye. Real-world ride-hailing vehicle repositioning using deep reinforcement learning. *Transportation Research Part C: Emerging Technologies*, 130:103289, 2021.

[86] Nandani Garg and Sayan Ranu. Route recommendations for idle taxi drivers: Find me the shortest route to a customer! In *Proceedings of the 24th ACM SIGKDD International Conference on Knowledge Discovery & Data Mining*, pages 1425–1434, 2018.

[87] Ashutosh Singh, Abubakr O Al-Abbasi, and Vaneet Aggarwal. A distributed model-free algorithm for multi-hop ride-sharing using deep reinforcement learning. *IEEE Transactions on Intelligent Transportation Systems*, 23(7):8595–8605, 2021.

- [88] Mingyue Xu, Peng Yue, Fan Yu, Can Yang, Mingda Zhang, Shangcheng Li, and Hao Li. Multi-agent reinforcement learning to unify order-matching and vehicle-repositioning in ride-hailing services. *International Journal of Geographical Information Science*, 37(2):380–402, 2023.
- [89] Yinquan Wang, Huijun Sun, Ying Lv, Ximing Chang, and Jianjun Wu. Reinforcement learning-based order-dispatching optimization in the ride-sourcing service. *Computers & Industrial Engineering*, 192:110221, 2024.
- [90] Jiekun Feng, Mark Gluzman, and Jim G Dai. Scalable deep reinforcement learning for ride-hailing. In *2021 American Control Conference (ACC)*, pages 3743–3748. IEEE, 2021.
- [91] Martin L. Puterman. *Markov Decision Processes: Discrete Stochastic Dynamic Programming*. John Wiley & Sons, Inc., USA, 1st edition, 1994. ISBN 0471619779.
- [92] Jim Dai, Manxi Wu, and Zhanhao Zhang. Optimal control of multiclass queueing networks using atomic action decomposition. *(Working Paper)*, 2025.
- [93] DOE. Alternative fuel station locator. <https://afdc.energy.gov/stations/#/corridors>, 2023. Accessed: 2023-06-04.
- [94] Chris Nelder and Emily Rogers. Reducing ev charging infrastructure costs. <https://rmi.org/wp-content/uploads/2020/01/RMI-EV-Charging-Infrastructure-Costs.pdf>, 2020.